

# Gallardo's Thesis

Gallardo Guillermo

September 14, 2018



# Contents

---

<b>Dedications</b>	vii
<b>1 Introduction</b>	1
1.1 Organization . . . . .	1
<b>2 The Human Brain: Context, Cellular Composition and Anatomy</b>	3
2.1 The Human Nervous System . . . . .	3
2.2 A Microscopic View of the Human Brain . . . . .	4
2.2.1 Neurons . . . . .	4
2.2.2 Neuroglial . . . . .	5
2.2.3 Neuronal Organization: Cortical Layers . . . . .	6
2.3 A Macroscopic view of the Human Brain . . . . .	6
2.3.1 Anatomy of the Gray Matter . . . . .	6
2.3.2 Anatomy of the White Matter . . . . .	7
2.3.3 Neuroanatomical Naming Conventions . . . . .	7
2.4 Cytoarchitectonics . . . . .	8
2.5 Brain Function . . . . .	8
2.5.1 Frontal Lobe . . . . .	8
2.5.2 Parietal Lobe . . . . .	9
2.5.3 Occipital Lobe . . . . .	9
2.5.4 Temporal Lobe . . . . .	9
2.5.5 Insula . . . . .	10
<b>3 Magnetic Resonance Imaging: A Non-invasive Study of Brain's Anatomy, Connectivity and Function</b>	13
3.1 Magnetic Resonance Imaging . . . . .	13
3.1.1 Nuclear Magnetism . . . . .	13
3.1.2 Magnetic Resonance Imaging Scanner . . . . .	14
3.2 Diffusion Magnetic Resonance Imaging . . . . .	16
3.2.1 Pulsed Gradient Spin Echo (PGSE) . . . . .	16
3.2.2 subsection . . . . .	17

## CONTENTS

---

3.3 Tractography . . . . .	18
3.4 fMRI . . . . .	20
<b>4 Mapping the Brain: A review of the brain divisions</b>	<b>23</b>
4.1 Overview . . . . .	23
4.2 Introduction . . . . .	23
4.3 All . . . . .	23
4.4 Cythoarquitecture . . . . .	23
4.5 Anatomical . . . . .	24
4.6 Functional . . . . .	24
4.6.1 Anatomical + Cythoarchitectural . . . . .	24
4.6.2 EEG . . . . .	24
4.6.3 fMRI . . . . .	24
4.7 Brain Networks . . . . .	25
4.8 Semantic . . . . .	25
4.9 Structural Connectivity . . . . .	25
4.10 Multimodal . . . . .	25
4.11 Discussion . . . . .	25
4.12 Resume of all of the parcellations presented . . . . .	26
4.13 Conclusion . . . . .	26
<b>5 Groupwise Structural Parcellation of the Whole Cortex: A Logistic Random Effects Model Based Approach</b>	<b>27</b>
5.1 Overview . . . . .	27
5.2 Introduction . . . . .	27
5.3 Methods . . . . .	29
5.3.1 Cortical Connectivity Model and Tractography . . . . .	29
5.3.2 Single Subject and Groupwise Parceling Methodologies . . . . .	30
5.4 Experiments and Results . . . . .	31
5.4.1 Data and Preprocessing . . . . .	32
5.4.2 Parcelling Subjects From the Human Connectome Project . . . . .	32
5.4.3 Groupwise Parcellation Technique Consistency . . . . .	32
5.4.4 Relationship with a Frontal Lobe Parcellation . . . . .	35
5.4.5 Anatomical Relationship and Functional Specialization of Our Parcels . . . . .	37
5.4.6 Relationship with a Multi-Modal Parcellation of the Cortex . . . . .	41
5.5 Discussion . . . . .	42

5.5.1	Our Groupwise Parcellations are Consistent Across Similar Groups: . . . . .	44
5.5.2	Our Method Creates Parcels in Agreement With a Single-Lobe Parcelling Technique Extant in the Literature. . . . .	45
5.5.3	Our Method Creates Several Parcels in Agreement with Brain Anatomy. . . . .	45
5.5.4	Our Results Show a Close Relationship Between Structural Connectivity and Brain Function. . . . .	47
5.5.5	Our Parcels Are Not Similar to Those Obtained by Glasser et al. (2016) But Possess Better Functional Specialization for Motor Tasks. . . . .	47
5.6	Conclusion . . . . .	47
<b>6</b>	<b>Solving the Cross-Subject Parcel Matching Problem using Optimal Transport</b>	<b>53</b>
6.1	Overview . . . . .	53
6.2	Introduction . . . . .	53
6.3	Methods . . . . .	54
6.3.1	Discrete Regularized Optimal Transport . . . . .	55
6.3.2	Matching Parcels Based on Dissimilarity Between Features . . . . .	56
6.4	Experiments and Results . . . . .	57
6.4.1	Data and Preprocessing . . . . .	57
6.4.2	Matching Parcels . . . . .	57
6.5	Discussion . . . . .	59
6.6	Conclusion . . . . .	59
<b>7</b>	<b>Inferring the Localization of White-Matter Tracts using Diffusion Driven Label Fusion</b>	<b>63</b>
7.1	Overview . . . . .	63
7.2	Introduction . . . . .	63
7.3	Methods . . . . .	64
7.3.1	Estimating an Orientation Density Function from dMRI Data . . . . .	64
7.3.2	Estimating an Orientation Density Function from Streamlines . . . . .	64
7.3.3	Label fusion . . . . .	65
7.4	Experiments and Results . . . . .	66
7.4.1	Data and Preprocessing . . . . .	66
7.4.2	Assessing goodness of the technique in synthetic data . . . . .	66
7.4.3	Assessing goodness of the techniques in real data . . . . .	66
7.4.4	Simulating Lesions in the White-Matter . . . . .	67
7.4.5	Discussion . . . . .	67
7.4.6	Conclusions . . . . .	67

## CONTENTS

## **Dedications**

---

To my family, with love

0. DEDICATIONS

# Chapter 1

## Introduction

---

The human brain is the most complex biological machine known in the universe. The brain works as a complex network of billion of neurons. Since this is impossible to handle, we need to subdivide the brain. Depending how you look at it, the brain can be divided following many different criteria (cytho, function). In each one of these criteria, brain connectivity is quite important and consistent. We know this thanks to invasive stuff. Since our brain is the result of biological evolution, we tortured monkeys, cats and rats in order to study and understand it. We cannot do that anymore, so it's difficult to study brain connectivity. Diffusion MRI allows to study the brain invivo without inducing pain/problems. But it has strong limitations: resolution in time and space, directionality, etc. It has been used to divide the brain, but the techniques are not good enough. We don't know how many parcels we need, or how to do it. We propose a parcellation technique that solves many of these problems. We show it is consistent with function. Now we would like to use this to study brain connectivity and function in different subjects. However, an interesting problem is that, for some regions, as frontal cortex, there's a lot of across subject variability. Turns out that it's hard to match parcels across subjects. Spatial overlap does not work here because of [cite]. We need to match stuff while imposing few constraints, specially spatial ones. The existing techniques are nice and simple, but not sufficient. We propose to improve the matching by using optimal transport. It actually works well. Now that we have a way to parcellate the brain, and a way to map that across subjects, maybe we can better study the structure-function relationship. I would like to talk about predicting function from structure. This would be a negative chapter, since we were not able to predict anything from tractography. But, what happens when there's a pathology in the white matter? It's affecting brain function, but we cannot precisely predict what since it impedes tractography. In that case, we need to do something to infer which bundles are affected.

We can do multi-atlas stuff. Since bundles are related to dmri, we can add dMRI information to the multi-atlas to improve the localization of affected bundles. Finally, the structure vs function in the brain does not necessarily always have to be structural connectivity vs tfmri function. We can also use microstructure vs cognitive, and microstructure to function (collaboration with vinod)

### 1.1. Organization

---

I start by making a beautiful introduction to neuroanatomy, because the reader needs to know what is a brain. Here we talk about sulci, giri, white matter, gray matter, cellular composition, layers, etc. This chapter also talks about brain function, but from an old perspective. Then, I move to explain the state of the art of the non-invasive techniques that we're interested in. Since the thesis is going to be about brain parcellation, I have to explain why we are interested on it. So the next chapter is about well known parcellations: cytho, broadmann areas, desikan, functional... the classical ones. Then, I can basically take the paper of Vinod and explain that, even when we subdivide the brain in specific areas, the brain works as a network. There should be a big focus on Structural connectivity since it's the main theme of the thesis. We start again with why structural connectivity is important. Then, we explain again that it's important to divide the brain based on its connectivity, so we know the basic pieces of the brain that work together. We present my work (CDMRI + neuroimage), this includes state of the art, and I guess stuff that was made after. Now, other chapter, we discuss that there's variability in the parcellation of different subjects. We insist in the fact that this is ok, because we are all different humans. Then we present the MICCAI paper made in collaboration with Nathalie, this includes state of the art, etc etc etc Another chapter, this time about multiatlas. Finally, something about structure vs

## 1. INTRODUCTION

function. In the intro we explained that structure is important, and that function is driven by function. It's time to show that this actually happens, and in which cases. We can start talking about Osher and others, however this didn't work for us. I think it's important to say it. Then, I can include the final part of my neuroimage, where we show the parcels are functionally specialized. Maybe something about the work with Nathalie. Stanford stuff goes here I guess

# Chapter 2

## The Human Brain: Context, Cellular Composition and Anatomy

### Overview

In this chapter we cover the basic aspects of cellular composition, morphology and function of the human brain. We start with a brief introduction to the human nervous system in order to understand the biological context of the brain. Then, we study the brain from both a microscopic and a macroscopic view. In the microscopic view, we explain the cellular composition of the brain and how it's organized. In the macroscopic view, we zoom out and make a review of the most important divisions and anatomical landmarks of the brain. Finally, we describe the functional role of some of these gross anatomical divisions. This chapter is heavily based on the books: Neuroscience<sup>1</sup>; Clinical Neuroscience<sup>2</sup> and Atlas of Human Brain Connections<sup>3</sup>. We encourage the reader to further deepen each subject using those books.

### 2.1. The Human Nervous System

Every organ in our body works as part of a larger system of organs that interact following a common goal. Our brain, the main actor of this thesis, forms part of the nervous system, the system concerned with conscious life. The nervous system is the most complicated and highly organized of the various systems which make up the human body [GRAY]. It is the mechanism concerned with the analysis and integration of internal and external stimuli, and with the reactions and adjustments of the organism following them. It may be anatomically divided into two parts, central and peripheral. The central nervous system (CNS) consist of the brain and the spinal cord. The peripheral nervous system (PNS) consists of a series of nerves that link receptors on the body with the central nervous system. These nerves are associated with the functions of the special and general senses and

with the voluntary movements of the body. As a system, the PNS transmits stimuli from the environment to circuits within the spinal cord and the brain, which are integrated alongside internal stimuli in order to produce a response. This response travels back through the PNS and is translated into body movement or internal organs' adjustment (fig. 2.1).

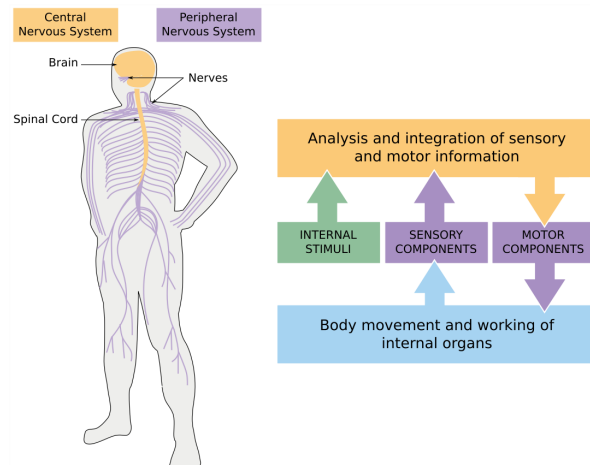


**Figure 2.1:** The two anatomical divisions of the nervous system and their functional relationship. Left. Simplified representation of the CNS and PNS in the human. Right. Diagram representing the interaction between both subnetworks. Internal and external stimuli gathered by the PNS are processed by the CNS, which decides how to respond.  
WE STOLE THIS IMAGE

In this thesis we will focus only on the brain, which constitutes the upper part of the central nervous system and regulates all human activity.

### 2.2. A Microscopic View of the Human Brain

## 2. THE HUMAN BRAIN: CONTEXT, CELLULAR COMPOSITION AND ANATOMY

---

posed by cells that can be divided in two broad categories: nerve cells (or neurons), and supporting cells called neuroglia (or simply glia). Nerve cells are discrete entities that communicate with one another by means of specialized contacts that Sherrington called synapses. [SHERRINGTON] Supporting cells, in contrast, are not capable of electrical signaling; nevertheless, they have several essential functions in the developing and adult brain. The human brain possess on average  $86.06 +/ - 8.12$  billion neurons and  $84.61 +/ - 2.17$  billion nonneuronal cells, making it a linearly scaled-up primate brain in its cellular composition. In terms of distribution, 80% of the neurons are present in the cerebellum, meanwhile only 19% of the nonneuronal are present there.

### Neurons

The basic cellular organization of neurons resembles that of other cells; however, they are clearly distinguished by specialization for intercellular communication. This attribute is apparent in their overall morphology, in the specific organization of their membrane components for electrical signaling, and in the structural intricacies of the contacts between neurons. The most obvious sign of neuronal specialization for communication via electrical signaling is the extensive branching of neurons. The most salient aspect of this branching for typical nerve cells is the elaborate arborization of dendrites that arise from the neuronal cell body (also called dendritic branches or dendritic processes). The spectrum of neuronal geometries ranges from a small minority of cells that lack dendrites altogether to neurons with dendritic arborizations that rival the complexity of a mature tree (see Figure 1.2). The number of inputs that a particular neuron receives depends on the complexity of its dendritic arbor: nerve cells that lack dendrites are innervated by (thus, receive electrical signals from) just one or a few other nerve cells, whereas those with increasingly elaborate dendrites are innervated by a commensurately larger number of other neurons. Nerve cells that carry information toward the brain or spinal cord (or farther centrally within the spinal cord and brain) are called afferent neurons; nerve cells that carry information away from the brain or spinal cord (or away from the circuit in question) are called effer-

ent neurons. Interneurons or local circuit neurons only participate in the local aspects of a circuit, based on the short distances over which their axons extend. These three functional classes—afferent neurons, efferent neurons, and interneurons—are the basic constituents of all neural circuits.

Cortical neurons can be divided in two major types: granule neurons and pyramidal neurons<sup>2</sup>.

Granule cells are star-shaped neurons with a typical diameter of less than  $20\mu\text{m}$ . They are multipolar neurons, this is, neurons that possess a single axon and many dendrites. Granule cells are either excitatory, which means they release the neurotransmitter glutamate to send signals to other cells, or inhibitory<sup>5</sup>, which means they release gamma-Aminobutyric acid to reduce neuronal excitability throughout the nervous system. Granule neurons mostly have purely intrinsic axons—they do not enter white matter and make only short-range, local connections.

Pyramidal neurons have large, pyramid-shape bodies that range from  $20-120\mu\text{m}$ . Pyramidal neurons are multipolar and excitatory neurons, and they comprise about two-thirds of all neurons in the mammalian cerebral cortex. On top of their numerical dominance, pyramidal neurons are also 'projection neurons', meaning that their axons are often 'extrinsic'—they make long connections through the white matter.

Another important type of neurons to this thesis are the spindle neurons<sup>2</sup>. Spindle neurons, also called von Economo neurons (VENs), are a specific class of neurons that are characterized by a large spindle-shaped soma (or body), gradually tapering into a single apical axon in one direction, with only a single dendrite facing opposite. VENs emerged within the last decade as having a potentially major role in self-awareness and social cognition in humans<sup>6</sup>.

### Neuroglial

Neuroglial cells are quite different from nerve cells. The major distinction is that glia do not participate directly in synaptic interactions and electrical signaling, although their supportive functions help define synaptic contacts and maintain the signaling abilities of neurons. Although glial cells also have

## 2. THE HUMAN BRAIN: CONTEXT, CELLULAR COMPOSITION AND ANATOMY

---

complex processes extending from their cell bodies, these are generally less prominent than neuronal branches, and do not serve the same purposes as axons and dendrites (Figure 1.5). The term *glia* (from the Greek word meaning glue) reflects the nineteenth-century presumption that these cells held the nervous system together in some way. The word has survived, despite the lack of any evidence that binding nerve cells together is among the many functions of glial cells. Glial roles that are well-established include maintaining the ionic milieu of nerve cells, modulating the rate of nerve signal propagation, modulating synaptic action by controlling the uptake of neurotransmitters at or near the synaptic cleft, providing a scaffold for some aspects of neural development, and aiding in (or impeding, in some instances) recovery from neural injury.

### Neuronal Organization: Cortical Layers

[JOHNS CLINICAL NEUROSCIENCE] More than 90% of the cerebral cortex has a characteristic six-layered structure that appeared with the evolution of the mammalian brain (Fig. 5.2). For this reason it is referred to as neocortex. Although the same six layers can be identified in all neocortical regions at some stage of development, they are not always present in the mature brain. The layer structure varies spatially in regard to cell organization (cytoarchitecture) and myelination (myeloarchitecture), defining distinct cortical areas which are likely to perform different functions.<sup>4,7</sup> Some regions of the cortex are referred to as agranular cortex since they have lost their internal granule cell layer.

### 2.3. A Macroscopic view of the Human Brain

---

Neurons never function in isolation; they are organized into circuits or structures that process specific kinds of information. The brain comprises a diverse collection of these neural structures, each with a distinctive shape and an intricate internal architecture. Brain tissue can be divided into grey and white matter. Grey matter is composed mainly of neuronal cell bodies, dendrites and synapses. It is sharply demarcated from the adjacent white mat-

ter, which is made up mostly of tightly packed axons travelling to other parts of the nervous system. The pale colour of white matter is due to the lipid-rich myelin sheath that surrounds axons and enhances their conduction velocity (see Fig. 1.9; see also Chs 5, 6).

### Anatomy of the Gray Matter

The cerebral cortex is the most important structure of the gray matter and plays a major role in cognitive functions. It is a layered sheet of tissue, 23 millimetres thick, highly convoluted. It's hypothesized that the mechanical tension created by neuronal connections, working against internally generated hydrostatic pressure, is a major driving force of these folds<sup>8</sup>. These convolutions allow a large surface area to fit within the available cranial volume. In particular, the human cerebral cortex attains a surface area of about  $1600\text{ cm}^2$ , nearly three times what it would be in the absence of convolutions 1, 2. This folding process creates grooves on the surface of the brain called sulci and ridges called gyri.

The cerebral cortex is divided in two hemispheres by a prominent central fissure. The hemispheres are characterized by the gyri (singular, gyrus) or crests of folded cortical tissue, and sulci (singular, sulcus) the grooves that divide gyri from one another. Although gyral and sulcal patterns vary from individual to individual, there are some fairly consistent landmarks, particularly the: central sulcus; lateral sulcus; parieto-occipital notch and pre-occipital notch. These landmarks help divide the hemispheres into four lobes: occipital, temporal, parietal, and frontal. Hidden from surface view is the insular lobe.

Other structures made of gray matter are the subcortical structures, named like this because they are in the white matter. Examples of them are the Thalamus, brainstem or hippocampus.

### Anatomy of the White Matter

[CATANI] Axons in the central nervous system are gathered into tracts that are more or less analogous to nerves in the periphery. Most of the cerebral fibers forming the white matter connect distant regions within the cortex. There are some fibers that,

## 2. THE HUMAN BRAIN: CONTEXT, CELLULAR COMPOSITION AND ANATOMY

---

although being located in the cerebral hemispheres do not connect the cortex, but only subcortical structures. Fibres group together to form bundles of different diameter and several bundles form larger pathways called fasciculi, or tracts. Some of these major bundles are well defined in the modern neuronanatomy.

Examples of major bundles in the human brain are the Corpus Callosum, the Internal Capsule and the Superior Longitudinal Fasciculus. The Corpus Callosum is the largest tract of the human brain, composed of some 200-300 million myelinated axons it connects both hemispheres, allowing to transfer information from one to another. The internal capsule contains ascending fibres mainly from the thalamus to the cortex, and descending fibres from the cortex to subcortical structures, and the spinal cord. This complex projection system conveys sensorial information to the cortex and controls movement. The Inferior Longitudinal Fasciculus is a tract with long and short fibres connecting the occipital and temporal lobes. It is involved in visual and language functions.

### Neuroanatomical Naming Conventions

Brain's anatomy is described from its surface, by means of orthogonal sections and tract dissections [Catani's book].

The surface of the brain can be viewed from the side (lateral view), the middle (medial view), the front (anterior or frontal view), and the back (posterior or occipital view). The same terminology is used to indicate different regions of the brain surface (e.g. dorso-lateral prefrontal cortex).

Sectional neuroanatomy describes the relationship between cortical and subcortical structures, most commonly visualized along orthogonal axial, coronal, and sagittal planes. In radiological convention, the axial slices are viewed from the feet towards the head. The coronal planes are conventionally oriented with the left side of the brain on the right side of the page (frontal view). Finally, the sagittal plane divides the brain into two hemispheres.

Connectional neuroanatomy delineates the origin, course, and termination of connecting pathways. The tracts are classified according to

their course and terminal projections. Commissural pathways run along a horizontal axis and connect the two hemispheres. The majority of the projection pathways have a perpendicular course along a dorso-ventral (descending) or ventro-dorsal (ascending) axis and connect the cerebral cortex to subcortical nuclei, cerebellum, and the spinal cord. The association tracts run longitudinal along an antero-posterior axis and connect cortical areas within the same hemisphere.

This rudimentary description of some prominent anatomical landmarks provides a framework for understanding how neurons resident in a number of widely distributed and distinct brain structures communicate with one another to define neural systems dedicated to encoding, processing and relaying specific sorts of information about aspects of the organism's environment, and then initiating and coordinating appropriate behavioral responses.

### 2.4. Cytoarchitectonics

---

The cerebral cortex is divided into more than fifty regions based on its cellular composition under the microscope. The most known and frequently cited cytoarchitectural organization is that of Brodmann [BRODMANN]. [Figure of Brodmann around here]

### 2.5. Brain Function

---

#### [CLINICAL NEUROSCIENCE]

While the cerebral hemispheres are specialized to carry out particular cognitive functions, which are said to be lateralized, each lobe has a main role. Here we present the general function of each lobe, while introducing some of their most important functional subdivisions. Once again, we do not give a lot of details, but only focus in which is most important for this thesis.

#### Frontal Lobe

The frontal lobe, responsible for motor functions, speech production, personality, insight and foresight;

The precentral gyrus, immediately anterior to the

## 2. THE HUMAN BRAIN: CONTEXT, CELLULAR COMPOSITION AND ANATOMY

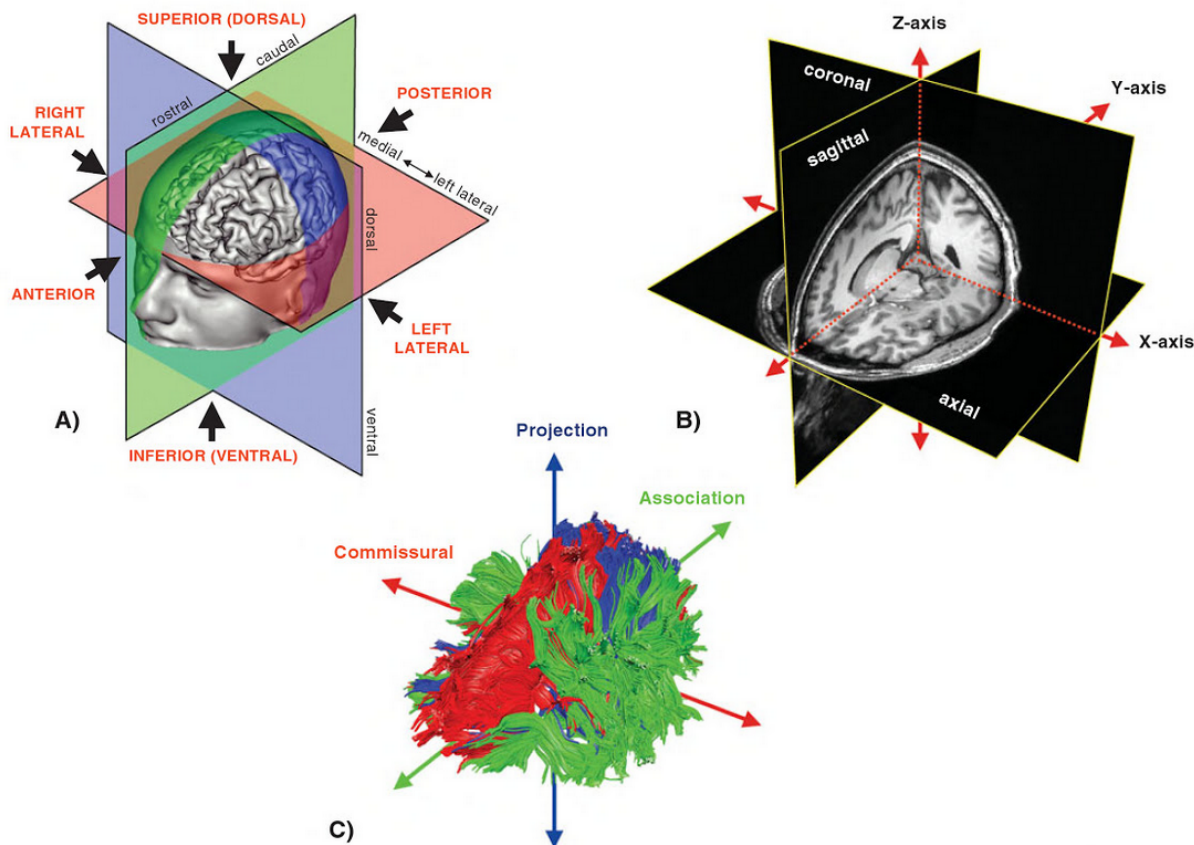


**Figure 2.2:** Terms commonly used to describe the orientation of the brain in surface (A), sectional (B) and connectional anatomy (C) representations.

central sulcus contains an inverted, point-to-point map of the motor functions of the opposite half of the body. This area is called primary motor cortex (BA 4). It was discovered by our dear friend Penfield. The representation of each body part in the motor strip is proportional to the precision of movement control. This means that the areas for the hands, face and tongue are disproportionately large [fig]. The region in front of the motor strip is the lateral premotor area (BA 6) but it does not correspond to any particular gyral or sulcal boundaries. The premotor cortex also contains an inverted body map and is concerned with preparation and execution of movement sequences in response to external stimuli (as catching a ball, rather than throwing one). More anteriorly, the frontal eye field (BA 8) is a cortical centre for attention and gaze which directs both eyes towards the contralateral visual

field. The large portion of the frontal lobe anterior to the motor and premotor areas is the prefrontal cortex and is involved in personality, behaviour, language and intellect. Its main concern is with organizing and planning behaviour in pursuit of short-, medium- and long-term goals. It also has a predominantly inhibitory role, preventing inappropriate behaviour [MARIANO SIGMAN]

Broca's area is involved in the expressive aspects of spoken and written language (production of sentences constrained by the rules of grammar and syntax). It corresponds to the opercular and triangular parts of the inferior frontal gyrus (BA 44 and 45) [FIGURE LANGUAGE]

### Parietal Lobe

## 2. THE HUMAN BRAIN: CONTEXT, CELLULAR COMPOSITION AND ANATOMY

---

The parietal lobe, responsible for language comprehension, spatial orientation and perception, and somatic senses, such as touch and temperature. The postcentral gyrus is immediately posterior to the central sulcus, behind and parallel to the motor strip. It corresponds to the primary somatosensory cortex (BA 3, 1 and 2). The sensory strip contains an inverted map of the opposite side of the body that mirrors that of the motor strip, but the relative proportions of the body parts reflect the degree of tactile sensitivity.

### Occipital Lobe

The occipital lobe is concerned entirely with visual processing and association. The retina contains a point-to-point (retinotopic) representation of the visual fields which is maintained throughout the central visual pathways. Posterior to the chiasm, the optic tracts continue on each side to the lateral geniculate nucleus (LGN) of the thalamus where they synapse. Thalamocortical neurons then project to the primary visual cortex, via the optic radiations. The central visual pathways are crossed. This means that the right visual field is represented in the left occipital lobe and vice versa. [Clinical neuroscience picture 3.7] The primary visual cortex is highly specialized for processing information about static and moving objects and is excellent in pattern recognition

### Temporal Lobe

The temporal lobe is involved in hearing, speech comprehension and visual recognition. The auditory cortex contains a tonotopic map that represents the audible frequency spectrum (low frequencies laterally, high frequencies medially). The fusiform gyrus (Latin: fusiform, shaped like a spindle) receives projections from the occipital lobe (part of the what pathway) and appears to be involved in the recognition of complex visual patterns. It contributes to reading (in the language-dominant hemisphere) and face recognition (in the non-dominant hemisphere).

Wernicke's area (pronounced: VER-nikker) corresponds to the posterior third of the superior temporal gyrus and is part of the auditory association cortex [FIGURE LANGUAGE], it's involved in transforming the visual impression of letters

(graphemes) into mental representations of speech sounds (phonemes).

### Insula

insular stuff

### Conclusions

---

This chapter introduced the basic knowledge in neuroanatomy necessary to understand the rest of the thesis. Moreover, it explained how the interaction between neurons by means of connectivity drives not only the brain morphology but also its function. This relationship between structural connectivity and morphology or function is one of the key aspect to explore and explode in this thesis.

Most of the content in this chapter has been acquired either postmortem, or using highly invasive techniques. In the next chapter, we show how the advances in quantum physics helped to develop Magnetic Resonance Imaging (MRI) and its derivates (Diffusion MRI and Functional MRI), in order to study the brain in a non-invasive way.

### Bibliography

---

- [1] D. Purves, G. J. Augustine, D. Fitzpatrick, W. C. Hall, A.-S. Lamantia, J. O. McNamara, and S. M. Willians, *Neuroscience*, vol. 3. 2004.
- [2] P. Johns, *Clinical Neuroscience*.
- [3] M. Catani and M. Thiebaut de Schotten, *Atlas of Human Brain Connections*. Oxford University Press, mar 2012.
- [4] M. D. Waehnert, J. Dinse, M. Weiss, M. N. Streicher, P. Waehnert, S. Geyer, R. Turner, and P. L. Bazin, "Anatomically motivated modeling of cortical laminae," *Neuroimage*, vol. 93, pp. 210–220, 2014.
- [5] J. M. Bekkers, "Pyramidal neurons," *Curr. Biol.*, vol. 21, no. 24, p. R975, 2011.
- [6] H. C. Evrard, T. Forro, and N. K. Logothetis, "Von Economo Neurons in the Anterior Insula of the Macaque Monkey," *Neuron*, vol. 74, no. 3, pp. 482–489, 2012.

---

## 2. THE HUMAN BRAIN: CONTEXT, CELLULAR COMPOSITION AND ANATOMY

- [7] S. T. Bok, “Der Einfluß der in den Furchen und Windungen auftretenden Krümmungen der Großhirnrinde auf die Rindenarchitektur.,” *Z. Gesamte Neurol. Psychiatr.*, vol. 121, no. 1, pp. 682–750, 1929.
- [8] D. C. Van Essen, “A tension-based theory of morphogenesis and compact wiring in the central nervous system,” 1997.

## 2. THE HUMAN BRAIN: CONTEXT, CELLULAR COMPOSITION AND ANATOMY

# Chapter 3

## Magnetic Resonance Imaging: A Non-invasive Study of Brain's Anatomy, Connectivity and Function

---

### Overview

Historically, the knowledge we possess of neuroscience has come from either studying brains post-mortem or by using heavily invasive techniques. The advent of Magnetic Resonance Imaging allowed to start studying the brain in a non-invasive way. Further technological advances opened the possibility of also studying brain function, and brain structure. In this chapter, we start by introducing some basic concepts in quantum physics and explain how they can be used to study the human brain. Then, we show how further improvements allow to estimate the location of tracts in the white-matter using Diffusion MRI. Finally, we make a brief introduction to how to detect functional specialization in the brain using Functional MRI. This chapter is strongly based on the book Diffusion MRI<sup>1</sup> and in the lessons of Dr. Michael L. Lipton available online<sup>2</sup>. Please refer to them in order to deepen on the subjects.

### 3.1. Magnetic Resonance Imaging

A little history about it. Lets say that it's amazing because you don't need to torture people. It works using principles of quantum physics.

#### Nuclear Magnetism

Atomic nucleus is. Atomic nucleus with a different number of neutrons and protons possess a non-zero spin, which is an intrinsic form of angular momentum. While there's not an actual movement, the spin can be interpreted as the particle spinning around its own axis<sup>3</sup>, since the spin behaves exactly like that. The nuclear magnetic moment is the magnetic moment of an atomic nucleus and arises from the spin of the protons and neutrons. If an atomic nucleus is placed inside of an external magnetic field, the spin of its protons will align with

the direction of the field. However, because of the spin angular momentum, the proton is forced out of the perfect alignment with the magnetic field, and starts to precess around the direction of the magnetic field, with some frequency and some angle (fig. X). The frequency with which the proton precess around the magnetic field is known as the Larmor frequency [REF], as is expressed as:

$$\omega = \vec{\mu} \times \vec{B} = \gamma \vec{J} \times \vec{B}. \quad (3.1)$$

where  $\vec{\mu}$  is the magnetic moment of the proton;  $\gamma$  is the gyromagnetic ratio of the proton;  $\vec{J}$  is its angular momentum and  $B$  is the gradient strength.

The angle at which the proton precess respect of the magnetic field depends on the amount of energy of the magnetic field. To more energy, more angle. This means that, given enough energy, it's possible to orientate the precessing in the direction transversal to the magnetic field. By placing a coil in the transversal plane, we can measure the voltage generated by the magnetic moment ( $|\mu|$ ) (Fig. 3.2). If the external magnetic field goes off, the voltage being measured in the transversal plane starts to evanescence. This is because the system starts to lose energy, and therefore, the angle between  $\mu$  and  $B$  decreases. This process is named relaxation.

The human body is composed by different types of tissue, each with its own chemical composition. Since different molecules possess different gyromagnetic ratio, each type of tissue will generate a different magnetic moment (eq. 3.1), and therefore, a different relaxation time. This means that if a person is placed inside of a magnetic field, different parts of the body will generate different magnetic moments. By placing a coil in the transversal plane, we could compare the different signals obtained. The problem is, that the amount of energy necessary to create a detectable precession would

### 3. MAGNETIC RESONANCE IMAGING: A NON-INVASIVE STUDY OF BRAIN'S ANATOMY, CONNECTIVITY AND FUNCTION

---

surely kill a human. Another way to increment the energy of the system is needed, and for this is that the concept of Resonance is used. Resonance is a phenomenon in which a system or external force drives another system to oscillate with greater amplitude at specific frequencies. In our case, we can generate external energy in the Larmor frequency of water (most important component), and the effect of Resonance will inject energy in the system.

#### Magnetic Resonance Imaging Scanner

A MR scanner is a machine able to create strong magnetic fields and radio frequency pulses in different frequencies. Particularly, while functioning a MR is constantly emitting an homogeneous magnetic field referred as  $B_0$  (Fig. 3.3). In order to obtain the relaxation time of a particular point in the body it uses gradient magnetic fields. A gradient is a magnetic field which strength varies linearly along a specific direction. When a gradient is applied, all the protons along its direction vary their Larmor frequency in a predictable way. By applying a gradient  $G_z$  in the  $z$  direction (Fig 3.4), the angular velocity of a proton respect to its position will be:

$$\omega(z) = B_z(z)g$$

This ensures us that if we apply a radio frequency (RF) pulse with a frequency of  $B_z(z_0)g$ , only the protons in the position  $z_0$  will resonate. Therefore, the signal obtained by the coil will only correspond to the protons in the slice at position  $z_0$ . It's important to state that, because of hardware limitations, it's impossible to generate a RF pulse in an exact frequency. What actually happens is that the pulse is generated for a small slice of frequencies, meaning that the protons in a small band around  $z_0$  will also resonate (Fig. X). This process is known as slice selection.

Once the desired slice is selected, we still need to apply two more gradients in order to recover the intensities at each point of the slide. So far, all of the protons inside of the slice are precessing in the same way. We can think of the slice as a two dimensional matrix, with two coordinates:  $x$  being the columns and  $y$  being the rows. The first

gradient is applied for a short period of time in one of the directions, lets say  $y$ . After the gradient is shutted down, the protons in each row will return to the same precessing velocity, but they'll have a different phase [FIG]. If then we apply a new gradient in the  $x$  direction, now it will happen that: the protons of each row will be oscillating in a different face, and the protons of each column will be oscillating at a different velocity. This means that, in our matrix, our information is encoded by phase in the rows and by velocity in the columns [FIG]. But when we take signal, we take signal for the whole column. We need to repeat this for different strengths of phase gradient  $G_x$ . Now we have a bunch of signals, that come from different frequencies (columns) and different strengths in the  $G_x$ , with greater and greater relative changes in phase. This is called k-space [REF] (<https://www.youtube.com/watch?v=wux9L8892KE>). Then you need to do a 2D fourier transform to recover the image.

#### 3.2. Diffusion Magnetic Resonance Imaging

---

The molecules inside a fluid in equilibrium are not still, on the contrary, they are randomly moving around. This physical phenomena is known as diffusion. Implications of diffusion in medicine.

In 1956, H.C. Torrey<sup>4</sup> observes that the magnetization can be lost by effect of diffusion. Somebody comes with a new idea of how to measure diffusion by introducing two new gradients. Let's explain the process in a intuitive way.

Imagine that after applying the RF pulse to do slice selection, we add a gradient field  $G_1 = G_d$  for a small time  $\delta ms$ . As explained in the previous section (sec. X), this will make the protons be off-phase between them. If after a  $\Delta$  time we apply the same gradient, but in the opposite direction  $G_2 = -G_d$ , also for  $\delta ms$ , then, the protons should go back to be in-phase [fig]. However, the particles undergoing diffusion will have moved (fig.), for which the second gradient  $G_2$  would have reached them in a different place, and therefore, change their angular velocity differently. In this way, a difference in the phase of the protons respect to the rest is a sign of diffusion [fig]. Since a voxel now

### 3. MAGNETIC RESONANCE IMAGING: A NON-INVASIVE STUDY OF BRAIN'S ANATOMY, CONNECTIVITY AND FUNCTION

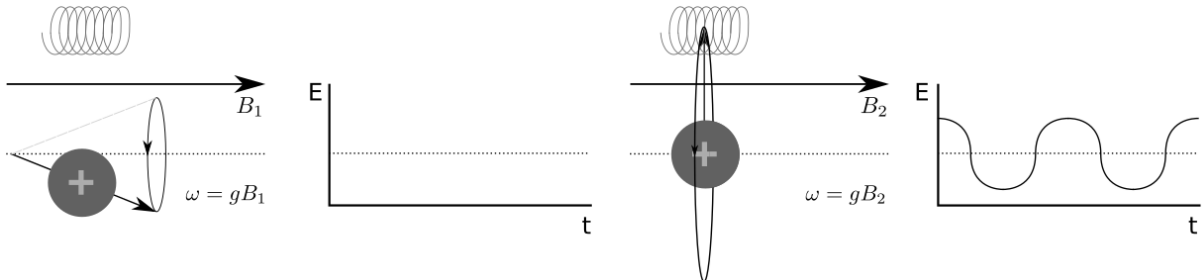


**Figure 3.1:** Spin under a weak electromagnetic field. The precessing happens close to the magnetic fields direction and the coil does not detect it.

**Figure 3.2:** After increasing the electromagnetic field, the precessing starts to move to the transversal plane, and the coil detects it.

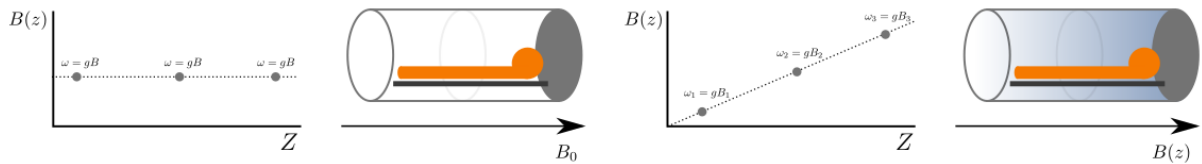


**Figure 3.3:** When protons a set of protons is placed inside an uniform magnetic field, they will all start to precess at the same velocity.

**Figure 3.4:** If a linear gradient magnetic field is applied, the velocity at which the protons precess will variate in a predictable way.

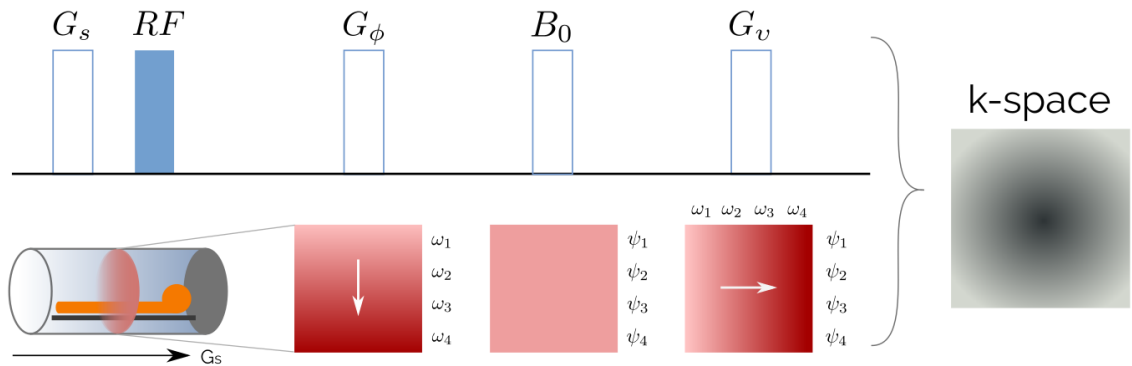


**Figure 3.5:** Pipeline of a Magnetic Resonance adquisition.

has protons precessing at different velocities, they create less signal. Max. signal is achieved when they all rotate together. The difference between the signal obtained with no diff. gradient and with

diff. gradient reflects the amount of diffusion.

#### Pulsed Gradient Spin Echo (PGSE)

### 3. MAGNETIC RESONANCE IMAGING: A NON-INVASIVE STUDY OF BRAIN'S ANATOMY, CONNECTIVITY AND FUNCTION

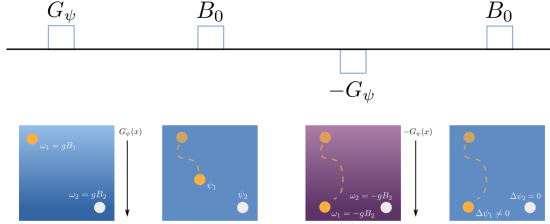


**Figure 3.6:** Figure explaining dMRI

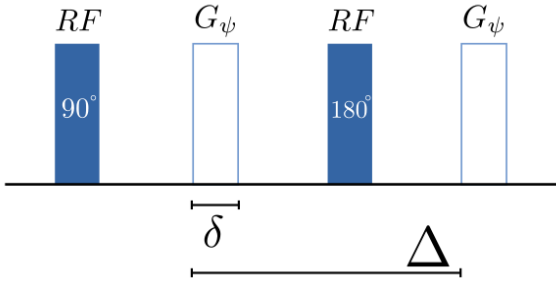


**Figure 3.7:** Secuencia Pulsed Gradient Spin Echo.

[refrase all] In 1965, Stejskal and Tanner invent the PGSE sequence to measure diffusion. The Stejskal-Tanner imaging sequence [Stejskal and Tanner (1965)] is used to measure the diffusion of water molecules in a given direction. This pulse sequence is illustrated in Figure 4.3. This sequence uses two gradient pulses in the direction  $g$ , of duration time  $\delta$ , to control the diffusion-weighting. They are placed before and after a 180 degrees refocusing pulse. More specifically, a first 90 degrees RF is applied to flip the magnetization in the transverse plane. The first gradient pulse causes a phase shift of the spins whose position are now a function of time. Spin position is in fact assumed to stay constant during time  $\delta$ . Finally, the 180 pulse combined with the second gradient pulse induces another phase shift. It is applied after a time separating the two gradient pulses. This pulse cancels the first phase shift only for static spins. On the other hand, spins under Brownian motion during the time period separating the two pulses undergo different phase shifts by the two gradient pulses, resulting in a T2 signal attenuation [Cercignani and Horsfield. (2001)]. By assuming the pulses to be infinitely narrow (narrow pulse approximation), i.e. if the gradient pulse duration  $\delta$  is short

enough for the diffusion of the water molecule to be negligible during that time, [Stejskal and Tanner (1965)] showed that the signal attenuation  $S(q_i)$  is expressed as the 3-dimensional (3D) Fourier transform  $F$  of the ensemble average propagator  $P$ ,

[some eq?]

where  $E(g, \delta, \Delta)$ ;  $g$  is the intensity of the gradient field;  $S_0$  is the signal obtained with no diffusion gradient ( $g = 0T/m$ ), and  $\gamma$  is the gyromagnetic ratio of water. Notice that we need  $S_0$  in the equation, since the diffusion comes from the difference in signal between the

Assuming the pdf to be gaussian, we get:

$$E(g, \delta, \Delta) = \frac{S(g, \delta, \Delta)}{S_0} = e^{-\gamma^2 g^2 \delta^2 (\Delta - \frac{\delta}{3}) D} \quad (3.2)$$

#### subsection

In 1985 Le Bihan<sup>5</sup> proposes to gather all the parameters in a single one:

$$b = \gamma^2 g^2 \delta^2 \left( \Delta - \frac{\delta}{3} \right)$$

, simplifying the equation 3.2 to:

$$E(b) = \frac{S(b)}{S_0} = e^{-bD}$$

where  $b$  represents the reciprocal of the diffusion intensity.

In 1994 Basser et al.<sup>6</sup> propose to measure the signal attenuation in different directions, and then approximate the diffusion coefficient with a second order tensor. A tensor is a multidimensional matrix associated to a base, which possess a transformation law indicating how the tensor components change when the base change. This sets the bases of what's known as DTI. DTI represents the diffusion as a 3-dimentional (3D) elipsoide, which can be coded in a symmetric matrix:

$$D = \begin{pmatrix} D_{xx} & D_{xy} & D_{xz} \\ D_{xy} & D_{yy} & D_{yz} \\ D_{xz} & D_{yz} & D_{zz} \end{pmatrix}$$

### 3. MAGNETIC RESONANCE IMAGING: A NON-INVASIVE STUDY OF BRAIN'S ANATOMY, CONNECTIVITY AND FUNCTION

---

Therefore we need at least 6 acquisitions.

One of the main limitants of this method is that it does not allow to represent the crossing of fibers. They get modeled as spheres.

In 1991 Callaghan et al.<sup>7</sup> developed the q-space analysis. This allows to make microscopy with dMRI. Based on the work of Stejskal and Tanner, Callaghan show that it's possible to express the signal attenuation as:

$$E(q, \Delta) = \frac{S(q, \Delta)}{S_0} = \int_{R^2} p(r; \Delta) e^{-2\pi i qr} dr$$
$$q = \frac{\gamma \delta g}{2\pi}$$

Where  $p(r; t)$  is the probability density that a set of particles travels a distance  $r$  during a time  $t$ . Because of this,  $p(r; t)$  is highly related to the compartment where the particles are contained.

One of the main advantages of q-space over DTI is that it does not assume any a prior model, allowing to define different strategies for  $p(r; t)$ . Here we talk about *Spherical Harmonics*<sup>8</sup> and *Constrained Spherical Deconvolution*<sup>9</sup>, which are the most relevant ones for this thesis.

#### 3.3. Tractography

---

Diffusion in the white matter is constrained by the tracts present on it. The protons present in any point of the brain will be able to diffuse only inside a tract and along its path. This means that, by following the diffusion signal, we should be able to trace the brain pathways. However, most of the methods to model diffusion signal cannot handle correctly the crossing of fibers. The best we can do, is to derive a probabilistic map from one voxel to another, and simulate the random movement of a water particle from one voxel to another. We hope that the diffusion signal + some constraints in the random walk allow us to retrieve the real pathways of the brain. Furthermore, if we generate a big number of this random walks, or streamlines, we hope to be able to recover the underlying tracts in a correct way by means of statistics. There are some issues with this. But there are some cool stuff about it also.

[VAN ESSEN] Using high-resolution postmortem diffusion imaging and tractography in Old World monkeys, we found a correlation coefficient of 0.58 between tractography-based and tracer-based estimates of connectivity; the correlation is highest for strong, short-distance pathways but is informative even for weak connections and widely separated areas (Donahue et al., 2016). We will discuss multiple reasons why tractography imperfectly reflects ground-truth neuroanatomical connectivity. This includes (i) a gyral bias in which tractography streamline within gyral blades are biased towards gyral crowns rather than sulcal banks (Van Essen et al., 2014); (ii) an anti-fundus bias in which connections to/from sulcal fundi tend to be obscured by tangential fiber bundles immediately subjacent to many sulci (Reveley et al., 2015); (iii) axonal branching within white matter that includes many branches at approximately right angles (Econo et al., 2016) that are inherently difficult to discriminate from crossing fibers that also occur within white matter; and (iv) potential dispersion or defasciculation in the white matter axonal trajectories of pathways that interconnect widely separated gray matter parcels (Jbabdi et al., 2015).

[MINE] A primary issue is the spatial resolution of diffusion imaging: it is several orders of magnitude coarser than axonal diameters (millimeters vs. micrometers) (Van Essen et al., 2014), making hard to infer some brain pathways. In addition, there is as yet no quantitative measure of the strength of connections from diffusion (Jbabdi and Behrens, 2013). Given a seed-point in the brain, probabilistic tractography creates a tractogram: an image where each voxel is valued with its probability of being connected to the seed through axonal bundles. One way of calculating these probabilities is with a Monte Carlo procedure, simulating the random walk of water particles through the white matter (Behrens et al., 2003). Each one of these paths is known as a streamline.

[MAXIME NATURE NEUROSCIENCE?] we organized an open international tractography challenge, which resulted in 96 distinct submissions from 20 research groups. To determine the current state of the art in tractography, we organized an international tractography competition and employed a novel validation method based on simulated DWI of a brainlike geometry. This ground truth data set

### **3. MAGNETIC RESONANCE IMAGING: A NON-INVASIVE STUDY OF BRAIN'S ANATOMY, CONNECTIVITY AND FUNCTION**

---

represented 25 wellknown valid bundles that covered approximately 70% of the human brain white matter.

While most stateoftheart algorithms reconstructed 90% of ground truth bundles to at least some extent, on average they produced four times more invalid than valid bundles. About half of the invalid bundles occurred systematically in the majority of submissions. The average ratio of false-positive to truepositive bundles was approximately four to one. This ratio could not be improved by employing higher quality data or even using the gold standard field of local orientations, highlighting that current tractography approaches are fundamentally illposed.

#### **3.4. fMRI**

---

<sup>10</sup> All the processes of neural signaling in the brain require energy in the form of adenosine triphosphate (ATP). When a region of the brain is up-regulated (i.e. activated) by a cognitive task such as finger tapping, the additional neural firing and other increased signaling processes result in a locally increased energy requirement. The brain responds by adjusting its blood flow to deliver nutrients such as oxygen and glucose to stressed tissues and allow them to function. Haemodynamic response (HR) allows the rapid delivery of blood to active neuronal tissues. The second mechanism, termed Blood Oxygenation Level Dependent (BOLD) contrast, was first demonstrated in rats<sup>48,50</sup> and later in humans<sup>3,37,49,52</sup>, and is the contrast that is used in virtually all conventional fMRI experiments. BOLD contrast results from the change in magnetic field surrounding the red blood cells depending on the oxygen state of the hemoglobin. When fully oxygenated, HbO<sub>2</sub> is diamagnetic and is magnetically indistinguishable from brain tissue. However, fully deoxygenated Hb has 4 unpaired electrons and is highly paramagnetic<sup>59</sup>. This paramagnetism results in local gradients in magnetic field whose strength depends on the [Hb] concentration. These endogenous gradients in turn modulate the intra- and extra-vascular bloods T2 and T2\* relaxation times through diffusion and intravoxel dephasing, respectively. Using a gradient refocused echo (GRE) MRI pulse se-

quence<sup>7</sup>, the acquisition is made sensitive to T2\* and T2. At 1.5T and 3T, the T2\* contrast is predominant and is largest in venules<sup>61</sup>, while at higher field strength the diffusion-weighted contrast of T2 relaxation becomes more important and, because signals are generated preferentially in capillaries and tissue with spin-echo acquisitions, provides greater spatial specificity<sup>57,64</sup>. Since most fMRI is currently performed at 3 Tesla or below, BOLD fMRI utilizes primarily GRE methods because of the increased T2\* contrast<sup>10</sup>.

[wikipedia et al.] Cerebral blood flow (CBF) is the blood supply to the brain in a given period of time.[ Tolias C and Sgouros S. 2006. "Initial Evaluation and Management of CNS Injury." ] The most common functional imaging signal is the blood-oxygen-level dependent signal (BOLD), which primarily corresponds to the concentration of deoxyhemoglobin.<sup>[12]</sup> The BOLD effect is based on the fact that when neuronal activity is increased in one part of the brain, there is also an increased amount of cerebral blood flow to that area which is the basis of haemodynamic response. This increase in blood flow produces an increase in the ratio of oxygenated hemoglobin relative to deoxygenated hemoglobin in that specific area. The difference in magnetic properties of oxygenated and deoxygenated hemoglobin is what allows fMRI imaging to produce an effective map of which neurons are active and which are not. In short, deoxygenated hemoglobin is paramagnetic while oxygenated hemoglobin is diamagnetic. Diamagnetic blood (oxyhemoglobin) interferes with the magnetic resonance (MR) signal less and this leads to an improved MR signal in that area of increased neuronal activity. However, Paramagnetic blood (deoxyhemoglobin) makes the local magnetic field inhomogenous. This has the effect of dephasing the signal emitted in this domain, causing destructive interference in the observed MR signal. Therefore, greater amounts of deoxyhemoglobin lead to less signal. Neuronal activity ultimately leads to an increase in local MR signaling corresponding to a decrease in the concentration of deoxyhemoglobin.<sup>[13]</sup>

### 3. MAGNETIC RESONANCE IMAGING: A NON-INVASIVE STUDY OF BRAIN'S ANATOMY, CONNECTIVITY AND FUNCTION

---

#### Conclusion

This chapter introduced the imaging techniques of MRI, Diffusion MRI and Functional MRI. These three methods provide means to study the brain anatomy, structure and function in a non-invasive way. Even when each technique has its own limitations, either in spatial or temporal resolution, they all allowed to highly advance the state of the art in neuroscience. In the next chapter we will see how these advances in imaging allowed to parcellate the brain, making it easier to study brain function.

#### Bibliography

- [1] P. J. Basser and E. Özarslan, “Introduction to Diffusion MR,” in *Diffus. MRI* (H. Johansen-Berg and T. E. J. Behrens, eds.), ch. 1, pp. 2–10, Academic Press, Inc., 2009.
- [2] M. L. Lipton, “Introducing MRI,” 2014.
- [3] M. SEGALA, “ABRAHAM PAIS, Niels Bohr’s Times, in physics, philosophy, and polity, Oxford, Clarendon Press, 1991, XVII + 565 pp. ill. (ISBN 0 19 852049 2).,” *Nunquam*, vol. 8, pp. 364–367, jan 1993.
- [4] H. C. Torrey, “Bloch Equations with Diffusion Terms,” *Phys. Rev.*, vol. 104, pp. 563–565, nov 1956.
- [5] D. Le Bihan and E. Breton, “Imagerie de diffusion in vivo par résonance magnétique nucléaire,” *Comptes rendus l’Académie des Sci. Série 2, Mécanique, Phys. Chim. Sci. l’univers, Sci. la Terre*, vol. 301, no. 15, pp. 1109–1112, 1985.
- [6] P. J. Basser, J. Mattiello, and D. Lebihan, “Estimation of the Effective Self-Diffusion Tensor from the NMR Spin Echo,” *J. Magn. Reson. Ser. B*, vol. 103, pp. 247–254, mar 1994.
- [7] P. T. Callaghan, A. Coy, D. MacGowan, K. J. Packer, and F. O. Zelaya, “Diffraction-like effects in NMR diffusion studies of fluids in porous solids,” *Nature*, vol. 351, pp. 467–469, jun 1991.
- [8] D. S. Tuch, “Q-ball imaging,” *Magn. Reson. Med.*, vol. 52, pp. 1358–1372, dec 2004.
- [9] J.-D. Tournier, F. Calamante, D. G. Gadian, and A. Connelly, “Direct estimation of the fiber orientation density function from diffusion-weighted MRI data using spherical deconvolution,” *Neuroimage*, vol. 23, pp. 1176–1185, nov 2004.
- [10] G. H. Glover, “Overview of functional magnetic resonance imaging,” *Neurosurg Clin N Am*, vol. 22, no. 2, pp. 133–139, 2011.

**3. MAGNETIC RESONANCE IMAGING: A NON-INVASIVE STUDY OF BRAIN'S ANATOMY, CONNECTIVITY AND FUNCTION**

---

# Chapter 4

## Mapping the Brain: A review of the brain divisions

---

### 4.1. Overview

---

The brain is composed of billions of neurons interacting at the same time between them. Given the complexity of this network, a dimensionality reduction is needed in order to study its properties. Since its beginning, neuroscientist have divided the brain based on different criteria. This allows to study the brain as a set of interacting regions, allowing to abstract the underlying neuronal complexity. However, it's not clear that a unique and truth division of the human brain exists. In this chapter, we make a review of the different type of parcellations that exist; explain their advantages, and the best scenarios where to use each.

### 4.2. Introduction

---

Subdividing the brain in regions homogeneous respect to some criteria is a necessary first step of every study in neuroscience. By doing this, it's not only possible to reduce dimensionality, but also to derive rules more general than when using the whole brain. How to divide the brain will heavily depend on the task desired to achieve. Using the wrong parcellation can introduce a bias in the results. Historically, the brain has been divided following different criteria. Furthermore, with every new technological advance, new parcellations arise. Perhaps the first parcellation to exist was the anatomical one. Still something from Demians thesis here. Based solely in the brain morphology, gross divisions of the brain can be made, as lobes and etc.

### 4.3. All

---

where I published mine:  
<https://www.sciencedirect.com/science/article/pii/S1053811917310091>  
Surface-Based and Probabilistic Atlases of Primate Cerebral Cortex David, in Mendeley.

### 4.4. Cythoarquitecture

---

Cythoarquitectonic divisions of the brain are based solely in the cellular composition of the cortex. In this atlases, a brain region possess the same cells inside of it. The first and most known division is that of Brodmann. Brodmann divided the brain in XX regions. He showed stuff for humans and animals. He showed relationship with function. Von Economo extended this work, and did more stuff. Someone showed that in this parcellation, the regions with similar cellular composition tend to be connected between them. in my mendeley<sup>1</sup>.

### 4.5. Anatomical

---

Anatomical divisions of the brain are based on the cortical morphology/shape.. check the name. The most know one is Desikan. Desikan is based on detecting a set of particular gyris, and then divide the brain based on them. It has XX divisions per hemisphere, is simmetrical and can be applied in monkeys also, I think.. check it. This map was further refined by Destrieux. Destrieux works in a similar way, but makes further subdivisions of giry and stuff. AAL is older than them? Anyway, no one recomends AAL.

<https://biomedia.doc.ic.ac.uk/brain-parcellation-survey/>

### 4.6. Functional

---

Functional subdivisions of the brain create maps of regions functionally specialized. This is, each region is in charge of a specific motor/cognitive function, or is part of a greater system with a specific functional goal.

Anatomical + Cythoarchitectural

The first functional maps where derived from lesions. Lessons in here determinated that function.

## 4. MAPPING THE BRAIN: A REVIEW OF THE BRAIN DIVISIONS

---

Lessons in there determined another one. Some activations while torturing cats also showed interesting stuff. Penfield + Knowledge of anatomy + broadman + broca + wernicke + etc There's a lot of information on diseases in the book Clinical Neuroscience, sounds like a good place to start

### EEG

No idea... i have to read it.  
<https://www.sciencedirect.com/science/article/pii/S1053811917307474>

### fMRI

With the invention of fMRI, it was possible to measure the level of oxygen in blood. Knowing that the neurons need oxygen as fuel to fire, we can find which region of the brain are being activated for specific tasks. Even more interesting is the fact that there are some regions that activate while in a resting state. Here we talk about many of them.

Good review in: <https://www.biorxiv.org/content/biorxiv/early/2017/06/06/135632.full.pdf>. Maybe precursor of this is anatomy+cytoarchitecture. But here we talk about really different modalities, as T1+T2+fMRI+goodknowswhat. We present at least two. I'm sure there are more. Parisot. Van Essen. ...?

### 4.7. Brain Networks

---

Vinod, brain as a system The lobes and subcortical structures do not function in isolation, in fact they are heavily connected through the fibre bundles which compose the white matter.

[VINOD] In his view, the human brain contains at least five major core functional networks: (i) a spatial attention network anchored in posterior parietal cortex and frontal eye fields; (ii) a language network anchored in Wernickes and Brocas areas; (iii) an explicit memory network anchored in the hippocampal-entorhinal complex and inferior parietal cortex; (iv) a face-object recognition network anchored in midtemporal and temporopolar cortices; and (v) a working memory-executive function network anchored in prefrontal and inferior parietal cortices.

Gael (which fmri clustering... in mendeley)  
<https://www.frontiersin.org/articles/10.3389/fnins.2014.00167/full>

### 4.8. Semantic

---

Semantic parcellations try to map semantic processing to the cortex. In this maps, a region of the brain is ligated to a specific 'definition?/semantic'.

<https://www.nature.com/articles/nature17637>  
Where Is the Semantic System? A Critical Review and Meta-Analysis of 120 Functional Neuroimaging Studies

### 4.9. Structural Connectivity

---

In a structural parcellation, regions have a homogeneous pattern of connectivity with the rest of the brain. The first maps come from tracers in monkey. The new ones come from tractography. Yeah, we know that tractography is not perfect, but we cannot torture any more monkeys. We name all of the principal players. Gallardo. Moreno-Dominguez. Alfred Awander PCA. Michel Thiebaut. Parisot.

### 4.10. Multimodal

---

Finally, more and more people is doing this. Maybe precursor of this is anatomy+cytoarchitecture. But here we talk about really different modalities, as T1+T2+fMRI+goodknowswhat. We present at least two. I'm sure there are more. Parisot. Van Essen. ...?

### 4.11. Discussion

---

There's not such a thing as a unique brain parcellation. While we cannot say that it doesn't exist. We know that all of our techniques have a limitation, either in resolution, SNR. At the same time, we cannot study things at the neuron level, because we have billions of neurons in the brain. It makes a lot of sense that each parcellation is different, because they're based in different criteria. Even when trying to parcellate data coming from a same machine (fmri, dmri, etc), changing the hypothesis will change the resulting parcellation. For example, in structural gradient vs structural parcel. The important thing is to be able to select the right parcellation for the right study.

---

## 4. MAPPING THE BRAIN: A REVIEW OF THE BRAIN DIVISIONS

---

### 4.12. Resume of all of the parcellations presented

---

Here I put a beautiful table resuming everything.

### 4.13. Conclusion

---

In order to reduce the complexity of the brain many studies start by subdividing the brain. Depending on the hypothesis driving the study, different type of parcellations can be used. In this chapter we presented parcellations based on different criteria: cytoarchitecture; anatomy, function, semantics and structural. We also presented some parcellation which are driven by a mixture of such criteria. Each parcellation possess its own advantages, and should be used in the right context. In the following chapter we will introduce the first contribution of this thesis: a technique to parcelate the cortex based on its structural connectivity. Our technique allows to create parcellations at the single-subject and group level, while having a good correlation with known divisions of the brain.

## Bibliography

---

- [1] G. H. Glover, “Overview of functional magnetic resonance imaging,” *Neurosurg Clin N Am*, vol. 22, no. 2, pp. 133–139, 2011.

#### 4. MAPPING THE BRAIN: A REVIEW OF THE BRAIN DIVISIONS

# Chapter 5

## Groupwise Structural Parcellation of the Whole Cortex: A Logistic Random Effects Model Based Approach

---

### 5.1. Overview

So far in this thesis we have introduced the necessary concepts in neuroanatomy; non-invasive imaging techniques to study the brain, and brain parcellation. In the first chapter we explained the importance of brain connectivity and its relation to brain function. On the second chapter, we explained how to estimate brain connectivity and brain function in a non-invasive way. The third chapter showed the ongoing effort to find new and relevant ways to divide the brain, in order to improve the way to study it. In particular, all of the parcellations based on structural connectivity are computationally expensive; need tuning of several parameters or rely on ad-hoc constraints. Furthermore, none of these methods present a model for the cortical extrinsic connectivity of the cortex. In this chapter, we propose a parsimonious model for the extrinsic connectivity and an efficient parceling technique based on clustering of tractograms. Our technique allows the creation of single subject and groupwise parcellations of the whole cortex. We show that our technique creates parcellations in agreement with anatomical, structural and functional parcellations extant in the literature.

This work has been published in the journal *Neuroimage*<sup>?</sup>

### 5.2. Introduction

The human brain is arranged in areas based on criteria such as cytoarchitecture, functional specialization or axonal connectivity<sup>1;2;3</sup>. Parcelling the cortex into such areas and characterizing their interaction is key to understanding how the brain works. Nowadays it is accepted that axonal connectivity plays a fundamental role in the interaction

between brain regions<sup>4</sup>. Moreover, current theories hold that long-range physical connections through axonal bundles, namely *extrinsic connectivity*, are strongly related to brain function, for example, this has been shown in macaques<sup>5</sup>. Therefore, understanding how the cortex is arranged based on its extrinsic connectivity can provide key information in unraveling the internal organization of the brain.

Diffusion MRI (dMRI) enables the *in vivo* exploration of extrinsic connectivity and other aspects of white matter anatomy on the brain. However, in using diffusion MRI to infer long-distance connectivity, several challenges arise. A primary issue is the spatial resolution of diffusion imaging: it is several orders of magnitude coarser than axonal diameters (millimeters vs. micrometers)<sup>6</sup>, making hard to infer some brain pathways. In addition, there is as yet no quantitative measure of the strength of connections from diffusion<sup>7</sup>. Given these general limitations, obtaining a cortical parcellation based on extrinsic connectivity remains challenging<sup>6;7</sup>. Moreover, most current parceling techniques compute either single-subject or groupwise parcellations. Single-subject techniques work by refining other parcellations<sup>8</sup>, which introduces a bias in the resulting parcellation; parceling only part of the cortex<sup>9;10;11;3</sup> or using ad-hoc metrics to compare extrinsic connectivity<sup>12</sup>. Meanwhile, existing groupwise methods rely on average connectivity profiles<sup>8;13</sup>, which prevents obtaining single subject parcellations; seek a matching across subjects after independent parcellations<sup>12</sup>, relying on possible noisy results, or need fine tuning of parameters, as the expected number of clusters to find<sup>14</sup>.

In this work, we present a parsimonious model for the cortical connectivity alongside an efficient parceling technique based on it. We summarize both contributions in Fig. 5.1. Our model assumes that the cortex is divided in patches of homoge-

## 5. GROUPWISE STRUCTURAL PARCELLATION OF THE WHOLE CORTEX: A LOGISTIC RANDOM EFFECTS MODEL BASED APPROACH

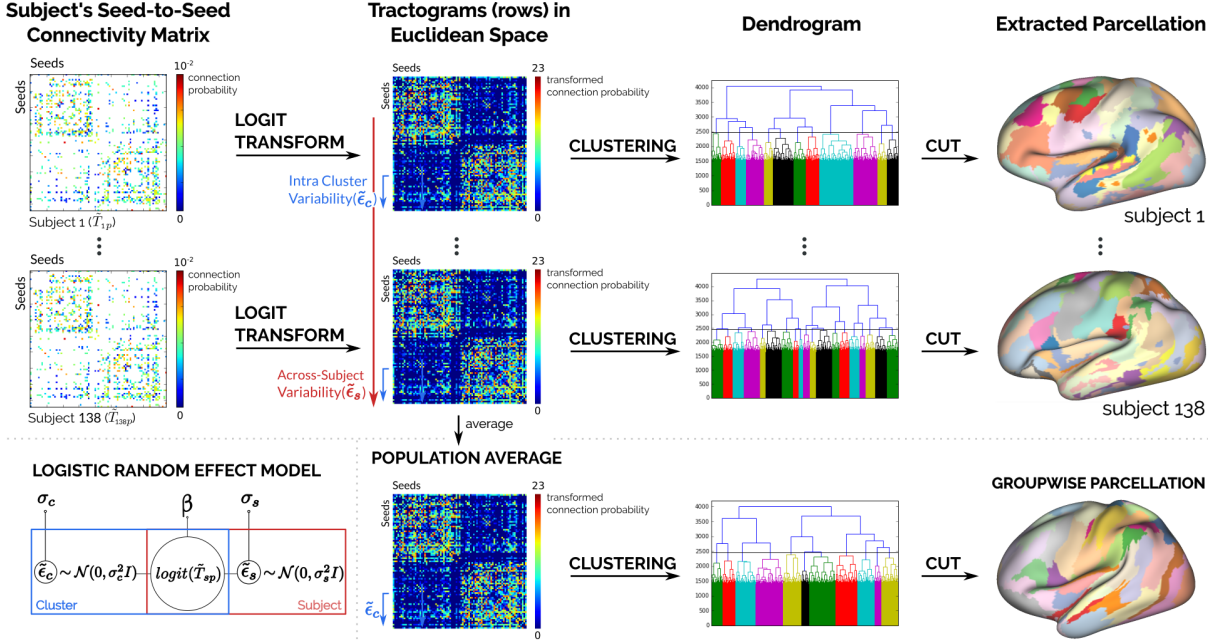


**Figure 5.1:** Lower left corner: graphical model of the linear relationship between the tractogram of a subject  $s$  for a seed  $p$  ( $\tilde{T}_{sp}$ ); and the intra-cluster ( $\bar{\epsilon}_c$ ) and across-subject ( $\bar{\epsilon}_s$ ) variability of the seed's patch. We transform the tractograms into a Euclidean space while explicitly accounting for the variability. This allows us to use well known clustering techniques and compress different levels of granularities for a same parcellation in a dendrogram.

neous extrinsic connectivity. That is, nearby neurons in the cortex share approximately the same long-range physical connections, we call this the *local coherence criterion*. Our assumption is based on histological results in the macaque brain<sup>4</sup>. Inspired by statistical models for clustered data<sup>15</sup>, our model accounts for the variability in the axonal connections of neurons within a patch and for variability in patch boundaries across subjects. Our parceling technique allows us to create single subject and groupwise parcellations of the whole cortex in agreement with extant parcellations.

We validate our technique by taking advantage of data available from the Human Connectome Project (HCP). Using our technique, we compute single subject and a groupwise parcellations. In this work we will focus on the groupwise case. For results of our method on the single-subject case please refer to ?. Here, we first assess the consistency of our groupwise parceling technique by comparing the groupwise parcellations of three disjoint groups of 46 subjects from the HCP. We also show that our technique computes a similar parcellation

to the one obtained by (author?)<sup>3</sup> when parcelling only the frontal cortex. Later, to test the functional specialization of our frontal lobe parcels, we use a data-base of meta-analysis of fMRI studies<sup>16</sup>, as in (author?)<sup>3</sup>. After, we show that our groupwise parcels subdivide some well-known anatomical structures by comparing our results against Desikan's atlas<sup>17</sup>. Also, we show the functional specialization of some of our parcels by comparing against results from (author?)<sup>18</sup>. Finally, we compare our groupwise parcellation of 138 subjects against the multi-modal parcellation of (author?)<sup>19</sup>. We show that, while the parcellations boundaries differ, our parcels show similar or better functional specialization, specially for motor related tasks.

This work is organized as follows: In the Methods section we present our model for cortical connectivity and frame tractography within our model. Also, we present both our single-subject and groupwise case methodologies to parcellate the cortex. In the Experiments and Results section we present our results on HCP data. We then discuss our results and

position ourselves with respect to the state of the art in the Discussion section. Finally, in the last section we provide our conclusions.

### 5.3. Methods

---

#### Cortical Connectivity Model and Tractogra-

Our model assumes that the cortex is divided in clusters of homogeneous extrinsic connectivity. That is, nearby neurons in the cortex share approximately the same long-ranged physical connections, we call this the *local coherence criterion*. Our assumption is based on histological results in the macaque brain<sup>4</sup>. As in clustered data models in statistics<sup>15</sup>, we allow intra-cluster and across-subject variability in the connectivity. We formalize this concept as:

$$K = \bigcup_{i=1}^k K_i, \forall 1 \leq i, j \leq k, i \neq j \rightarrow K_i \cap K_j = \emptyset \wedge \text{conn}(K_i) \neq \text{conn}(K_j)$$
(5.1)

where the set of points on the cortex  $K$  is the disjoint union of each cluster  $K_i$  and  $\text{conn}(\cdot)$  is the extrinsic connectivity fingerprint of a cluster. We will make the notion of variability explicit in eq. 5.3. In this work, the connectivity fingerprint of a seed-point in the brain is a binary vector denoting to which other seed-points it is connected through axonal bundles. That is, the physical connections of a point  $p \in K_i$  in the brain are represented by its connectivity fingerprint  $\text{conn}(p) = \text{conn}(K_i)$ .

Currently, the most common tool for estimating the extrinsic connectivity fingerprint of a point *in vivo* is probabilistic tractography<sup>7</sup>. Given a seed-point in the brain, probabilistic tractography creates a *tractogram*: an image where each voxel is valued with its probability of being connected to the seed through axonal bundles. One way of calculating these probabilities is with a Monte Carlo procedure, simulating the random walk of water particles through the white matter<sup>20</sup>. Each one of these paths is known as a streamline. If we model these streamlines as Bernoulli trials, where we get a value for the connection from our seed with other points (1 if they connected by the streamline, 0 if not)<sup>20</sup>, then, we can model the tractogram of the subject

$s$  in the seed-point  $p$  as:

$$T_{sp} = [P(\tilde{C}_{spi} = 1)]_{1 \leq i \leq n} = [\theta_{spi}]_{1 \leq i \leq n}, \quad \tilde{C}_{spi} \sim \text{Bernoulli}(\theta_{spi}),$$
(5.2)

where  $\tilde{C}_{spi}$  is a Bernoulli random variable<sup>1</sup> representing “the point  $p$  of the subject  $s$  is connected to the voxel  $i$ ”. Each Bernoulli’s parameter ( $\theta_{spi}$ ) represents the probability of being connected, and is estimated as the proportion of success in the Bernoulli trials of each seed.

To formulate the tractogram in accordance to our hypothesis of cortical connectivity, we model it as a vector of random variables. In our model, each element in a tractogram comes from a random variable depending on the point’s cluster along with its intra-cluster and across-subject variability:

$$p \in K_c \rightarrow \tilde{T}_{sp} = [P(\tilde{C}_{spi} = 1 | \text{conn}(K_c), \tilde{\epsilon}_{ci}, \tilde{\epsilon}_{si})]_{1 \leq i \leq n},$$
(5.3)

in this case, the point  $p$  belongs to the cluster  $c$ ;  $\tilde{\epsilon}_{ci}$  represents the intra-cluster variability and  $\tilde{\epsilon}_{si}$  represents the across-subject variability for the con-

~~neon(K<sub>i</sub>) voxel  $i$  in the cluster  $c$ .~~

Since each  $\tilde{C}_{spi}$  follows a Bernoulli distribution (Eq. 5.2) it is difficult to find an explicit formulation for  $P(\tilde{C}_{spi} = 1 | \text{conn}(K_c), \tilde{\epsilon}_{ci}, \tilde{\epsilon}_{si})$  accounting for the variabilities. For this, we use the generalized linear model (GLM) theory. In this theory, the data is assumed to follow a linear form after being transformed with an appropriate link function<sup>21</sup>. Using the following notation abuse:

$$\text{logit}(\tilde{T}_{sp}) \triangleq [\text{logit}(P(\tilde{C}_{spi} = 1 | \text{conn}(K_c), \tilde{\epsilon}_{ci}, \tilde{\epsilon}_{si}))]_{1 \leq i \leq n},$$
(5.4)

we derive from GLM a logistic random-effects model<sup>15</sup> for each point  $p$ :

$$\text{logit}(\tilde{T}_{sp}) = \beta_c + \tilde{\epsilon}_c + \tilde{\epsilon}_s \in \mathbb{R}^n, \quad \tilde{\epsilon}_c \sim \mathcal{N}(\vec{0}, \sigma_c^2 \text{Id}), \quad \tilde{\epsilon}_s \sim \mathcal{N}(\vec{0}, \sigma_s^2 \text{Id}),$$
(5.5)

where  $\epsilon_c$  and  $\epsilon_s$  represent the intra-cluster and across-subject variability respectively. According to GLM theory  $\beta_c \in \mathbb{R}^n$  is the extrinsic connectivity fingerprint of cluster  $K_c$  transformed:

$$\text{logit}^{-1}(\beta_c) = E(\tilde{T}_{sp}) = \text{conn}(K_c).$$
(5.6)

The choice of logit as link function is based on the work of **(author?)**<sup>22</sup>. In their work, **(author?)**<sup>22</sup>

<sup>1</sup>For the sake of clarity we denote all random variables with a tilde, e.g.  $\tilde{C}$ .

## 5. GROUPWISE STRUCTURAL PARCELLATION OF THE WHOLE CORTEX: A LOGISTIC RANDOM EFFECTS MODEL BASED APPROACH

---

show that logit function's codomain is a Euclidean space, which allows us to transform and manipulate the tractograms in a well-known space.

### Single Subject and Groupwise Parcelling

In the previous section, we hypothesized that the cortex is divided in clusters with homogeneous extrinsic connectivity, alongside intra-cluster and across-subject variability. In using the previous hypothesis, it is important to remark that we don't have a priori knowledge of the cluster's location or their variability. But, thanks to the proposed logistic random effects model, we formulated the problem of finding these clusters as a well-known clustering problem. This is because, after transforming the tractograms with the logit function as in eq. 5.4 they will be in a Euclidean space<sup>22</sup>. Even more, eq. 5.5 states that the transformed tractograms come from a mixture of Gaussian distributions, e.g. it is a Gaussian mixture model.

To solve the Gaussian mixture model and find the clusters, we use a modified Agglomerative Hierarchical Clustering (AHC) algorithm. This was inspired by the method of (author?)<sup>12</sup>. To enforce the local coherence criterion we also modify the algorithm to accept one parameter: the minimum size of the resulting clusters. Clusters smaller than this size are merged with neighbors, i.e. physically close clusters in the cortex. As we are working in a Euclidean space, we use Ward's Hierarchical Clustering method<sup>23</sup>. This method creates clusters with minimum within-cluster variance. The method's result is a dendrogram: a structure that comprises different levels of granularity for the same parcellation. This allows us to explore different parcellation granularities by choosing cutting criteria, without the need of recomputing each time.

The main advantage of the model we proposed in this work is that it allows us to create a groupwise parcellation using linear operations. Assuming direct seed correspondence across subjects, as in the HCP data set, our model lets us remove the subject variability of each seed's tractogram by calculating the expected value across subjects:

$$E_s(g(\tilde{T}_{sp})) = E_s(\beta_c + \tilde{\epsilon}_c + \tilde{\epsilon}_s), = \beta_c + \tilde{\epsilon}_c + E_s(\tilde{\epsilon}_s) = \beta_c + \tilde{\epsilon}_c \quad (5.7)$$

where the last equality is due to  $E_s(\tilde{\epsilon}_s) = 0$  (Eq. 5.5). Since in our model the variabilities are normally distributed (Eq. 5.5), we can estimate the expected value across subjects by averaging a seed's tractograms across subjects. This allows us to create population-representative tractograms for each seed free of across-subject variability, which then can be clustered to create a groupwise parcellation.

## 5.4. Experiments and Results

---

In the previous section we presented a model for the cortical extrinsic connectivity and a clustering technique to parcellate the whole brain. Our technique allows us to create single subject and groupwise parcellations, encoded with different levels of granularity in a dendrogram. Now, we show the results of applying our technique over the HCP dataset. First, we explain how the preprocessing step of tractography was made. Then, we elaborate in detail how we applied our technique. Later, we show that our groupwise technique creates results consistent when parcelling different groups. Also, we show that our techniques creates parcels in accordance with those by (author?)<sup>3</sup> when parcelling only the frontal lobe. Then, we present a proof-of-principle that our parcels are related to brain anatomy and functional specialization. Most of the results in this section are focused in the groupwise case, for further information on the single-subject technique please refer to ?. Finally, we study the (dis)similarity between our groupwise parcellation and that of (author?)<sup>19</sup>.

### Data and Preprocessing

#### Human Connectome Project Dataset

A total of 138 subjects (65 males and 73 females, ages 31-35) were randomly selected from the group S500 of the Human Connectome Project (HCP). For information on the acquisition protocols please refer to (author?)<sup>24</sup>. Every subject has been already preprocessed with the HCP minimum pipeline<sup>18</sup>. Also, each subject's cortical surface is coregistered and represented as a triangular mesh of approximately 32000 vertices per hemisphere<sup>18</sup>.

For each vertex, the corresponding label from Desikan's Atlas is known<sup>17</sup>. Finally, the group S500

## 5. GROUPWISE STRUCTURAL PARCELLATION OF THE WHOLE CORTEX: A LOGISTIC RANDOM EFFECTS MODEL BASED APPROACH

---

contains tfMRI information representing the average response to functional stimuli in 100 unrelated subjects (U100)<sup>25</sup>.

### Probabilistic Tractography

To create the tractograms of each subject, we performed Constrained Spherical Deconvolution (CSD) based tractography<sup>26</sup> from a dense set of points in the cortex. Specifically, since each subject has a mesh representing their gray-matter/white-matter interface<sup>18</sup>, we used their vertices as seeds to create tractograms. Vertices corresponding to the medial wall were excluded. To avoid superficial cortico-cortical fibers<sup>27</sup>, we shrank each of the 138 surfaces 2mm into the white matter. For each subject, we fitted a CSD model<sup>26</sup> to their diffusion data using Dipy (version 0.11)<sup>28</sup> and created 5000 streamlines per seed-voxel using the implementation of probabilistic tractography in Dipy. Later, we created a tractogram as in (Eq. 5.2) by calculating for each seed the fraction of they particles that visited other seed-voxel.

### Parcelling Subjects From the Human Connectome Project

After performing tractography, we applied our parcelling technique over each subject in our HCP sample. Specifically, we first transformed each tractogram with the logit function as in eq. 5.4. Then, we clustered the tractograms of each subject using the modified AHC algorithm while imposing a minimum cluster size of 3mm<sup>2</sup> in the finest granularity. To retrieve parcellations from the resulting dendrogram we use the horizontal cut method<sup>29;12?</sup>. Two examples of obtained single-subject parcellations at a granularity of 55 parcels are shown in fig. 5.2. To create the groupwise parcellation, we took advantage of the vertex correspondence across subjects in the HCP data set<sup>18</sup>. After transforming the tractograms with the logit transform, we computed the average connectivity of each seed by averaging its tractograms across-subject. Then, we computed the groupwise parcellation by clustering the averaged tractograms with our proposed technique (sec. 5.3.2). The obtained groupwise parcellation at a granularity of 55 parcels is shown in fig. 5.2.

### Groupwise Parcellation Technique Consistency

To study the consistency of our technique, we randomly divided our HCP subject sample in 3 disjoint groups, trying to maintain the same proportion of males and females on each. The resulting groups had: 24 females, 22 males (group A); 23 females, 23 males (group B) and 28 females, 18 males (group C). For each group we computed their groupwise parcellation. The resulting parcellations at two different levels of granularity are shown in fig. 5.3. To study the similarity between the obtained groupwise parcellations, we compared them at different levels of granularity using the adjusted Rand index<sup>30</sup>. To have a baseline for the comparisons, we generated random parcellations of the cortex and computed the similarity between them. We computed two types of random parcellations: The first one is an homogeneous random parcellation with  $n$  parcels, inspired in a method used by (author?)<sup>14</sup>. To compute it, we start by choosing  $n$  starting points in the cortex, then, we randomly expand each parcel on the cortex. By comparing these random parcellations between them we compute the minimum obtainable Rand index by mere chance at each level of granularity. In the second type of random parcellation, we simulate the behavior of our technique. For this, we create a parcellation with 300 parcels and then, we iteratively merge two parcels chosen at random until all the parcels are merged in one. By comparing these random parcellations between them we obtain the minimum obtainable Rand index by a random Hierarchical Clustering Algorithm. Examples of these random parcellations can be seen in Fig 5.4. The baselines presented in fig. 5.5 (yellow and violet lines) were computed by comparing 1000 of these random parcels at different levels of granularity. The result of comparing the groupwise parcellations of each group appear in fig. 5.5. The figure shows that the similarity between our groupwise parcellations (lines red, green and blue) are significantly higher than the baselines (violet and yellow). That is, the similarity between our parcellations differs (for most cases) more than 3 standard deviations from the baselines' mean. Moreover, the similarity between our results differs more than 4 standard deviations from the comparison between synthetic hierarchical parcels. This results show that

## 5. GROUPWISE STRUCTURAL PARCELLATION OF THE WHOLE CORTEX: A LOGISTIC RANDOM EFFECTS MODEL BASED APPROACH

---

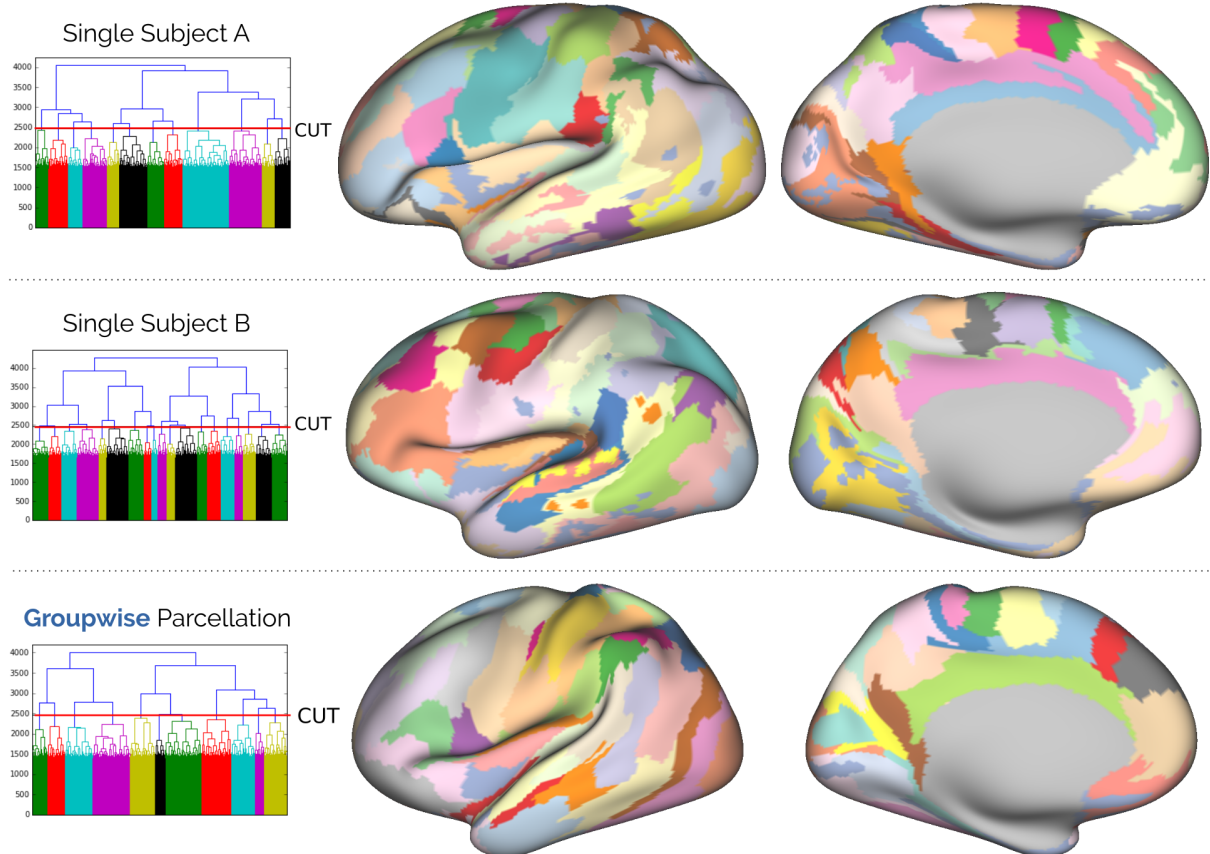


**Figure 5.2:** Examples of two single-subject parcellations and the groupwise parcellations computed with our technique. All the parcellations shown have 55 parcels. The corresponding dendrogram for each case, along with the chosen cut height (red line) are shown. The groupwise parcellation is based on 138 subjects from the Human Connectome Project.

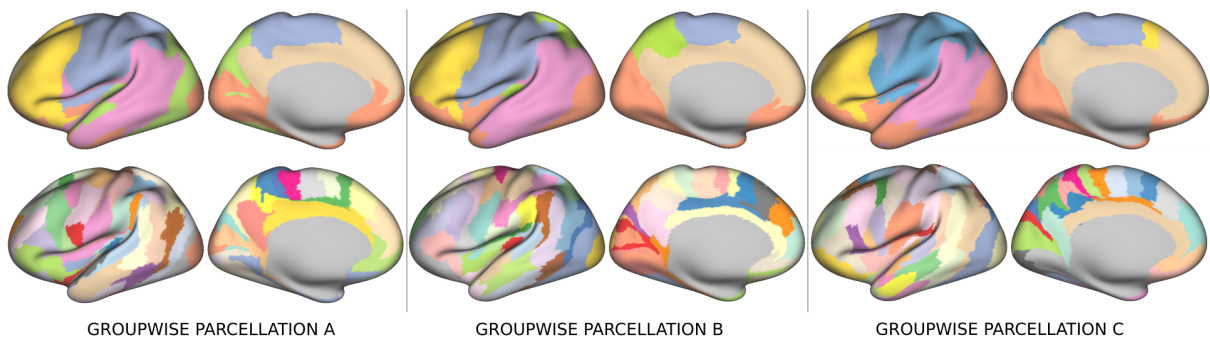


**Figure 5.3:** Groupwise parcellations of 3 disjoint groups of 46 people each. We show results from the same dendrogram cut to get 6 parcels (upper) and 55 parcels (lower). Labels with best overlap in upper figures share the same color. Notice that there are two different shades of blue for the group C.

## 5. GROUPWISE STRUCTURAL PARCELLATION OF THE WHOLE CORTEX: A LOGISTIC RANDOM EFFECTS MODEL BASED APPROACH

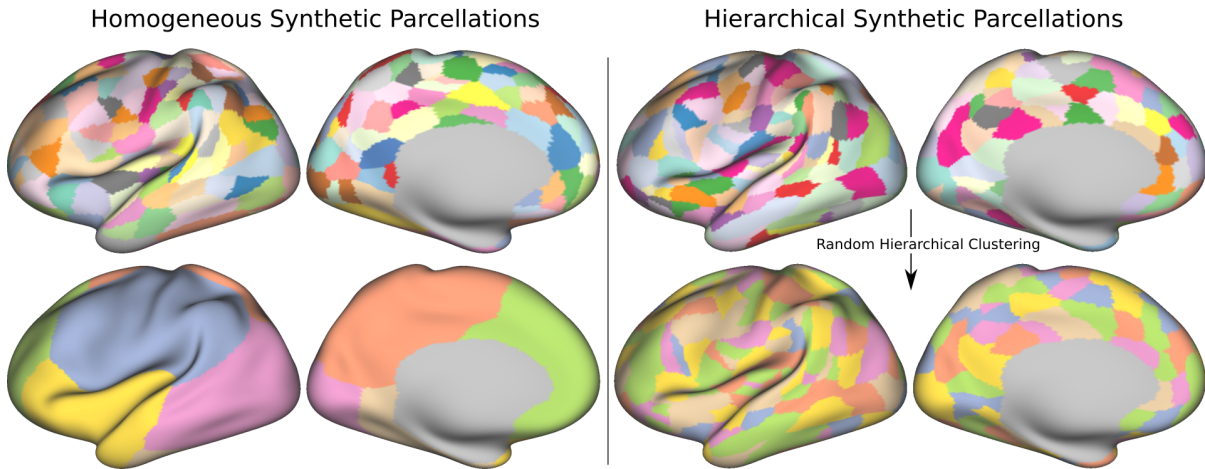


**Figure 5.4:** Examples of synthetic parcellations created to compute a baseline adjusted rand index. Parcellations on the left were created by dividing the brain in a homogeneous way, inspired by the random parcellation presented in (author?)<sup>14</sup>. Parcellations on the right were created by randomly merging parcels of a coarse parcellation.

our groupwise parceling technique creates consistent parcellations.

### Relationship with a Frontal Lobe Parcellation

Here we assess the agreement of our technique with an state-of-the-art extrinsic connectivity parcelling technique. We do so by using our technique to parcellate the frontal lobe and compare our result against that of (author?)<sup>3</sup>. In their work, (author?)<sup>3</sup> use a principal component analysis (PCA) statistical framework to parcellate the frontal lobe. They obtain a parcellation with 12 parcels. Then, they show that each one of these parcels possess a functional specialization by using the Decode tool<sup>2</sup> from Neurosynth<sup>16</sup>. Thiebaut's parcellation is currently available in Neurovault<sup>31</sup> as an annotated volume<sup>3</sup>, registered on the Colin27 template<sup>32</sup>. We downloaded this parcellation and projected its parcels into a dense mesh representing the cortex of the Colin27 template. The dense mesh had the same amount of vertices as our chosen HCP subjects, and such vertices were coregistered with the HCP subjects' cortical surfaces ones.

From the Desikan Atlas<sup>17</sup> of each of our HCP subjects, we derived a groupwise mask for the frontal lobe. Then, we computed a groupwise parcellation

with our technique, using only the tractograms in the mask. Figure 5.6 shows both the parcellation downloaded from Neurovault and our groupwise parcellation projected in the Colin template cortical surface. The figure shows our parcellation with 10 parcels since this level of granularity showed the best Rand index against the Thiebaut's parcellation. The colors of each parcel in our groupwise parcellation were picked in base to the position and amount of overlapping with the Thiebaut's parcels on the surface. While the similarity according to the Rand index is not significantly high (0.4), some visual similarity can be observed on the obtained parcellation, particularly in the blue, yellow, orange and green parcels. Moreover, as shown in table 1, our parcels show the same or even a higher level of functional specialization when processed with Neurosynth.

To study the consistency of our result we computed the frontal lobe groupwise parcellation in each of the 3 disjoint groups from the previous experiment. Figure 5.7 shows the three obtained parcellation alongside the Thiebaut's one. The obtained parcels show consistency, obtaining an adjusted Rand index score of  $0.61 \pm 0.05$  between them. Finally, we studied if the masking affected the clustering of the frontal lobe. To do so, we applied the frontal lobe mask over a groupwise whole-brain parcellation of the 138 subjects. The resulting frontal lobe parcellation contained 12 parcels. This parcella-

<sup>2</sup><http://www.neurosynth.org/decode/>

<sup>3</sup><http://neurovault.org/collections/1597/>

## 5. GROUPWISE STRUCTURAL PARCELLATION OF THE WHOLE CORTEX: A LOGISTIC RANDOM EFFECTS MODEL BASED APPROACH

---

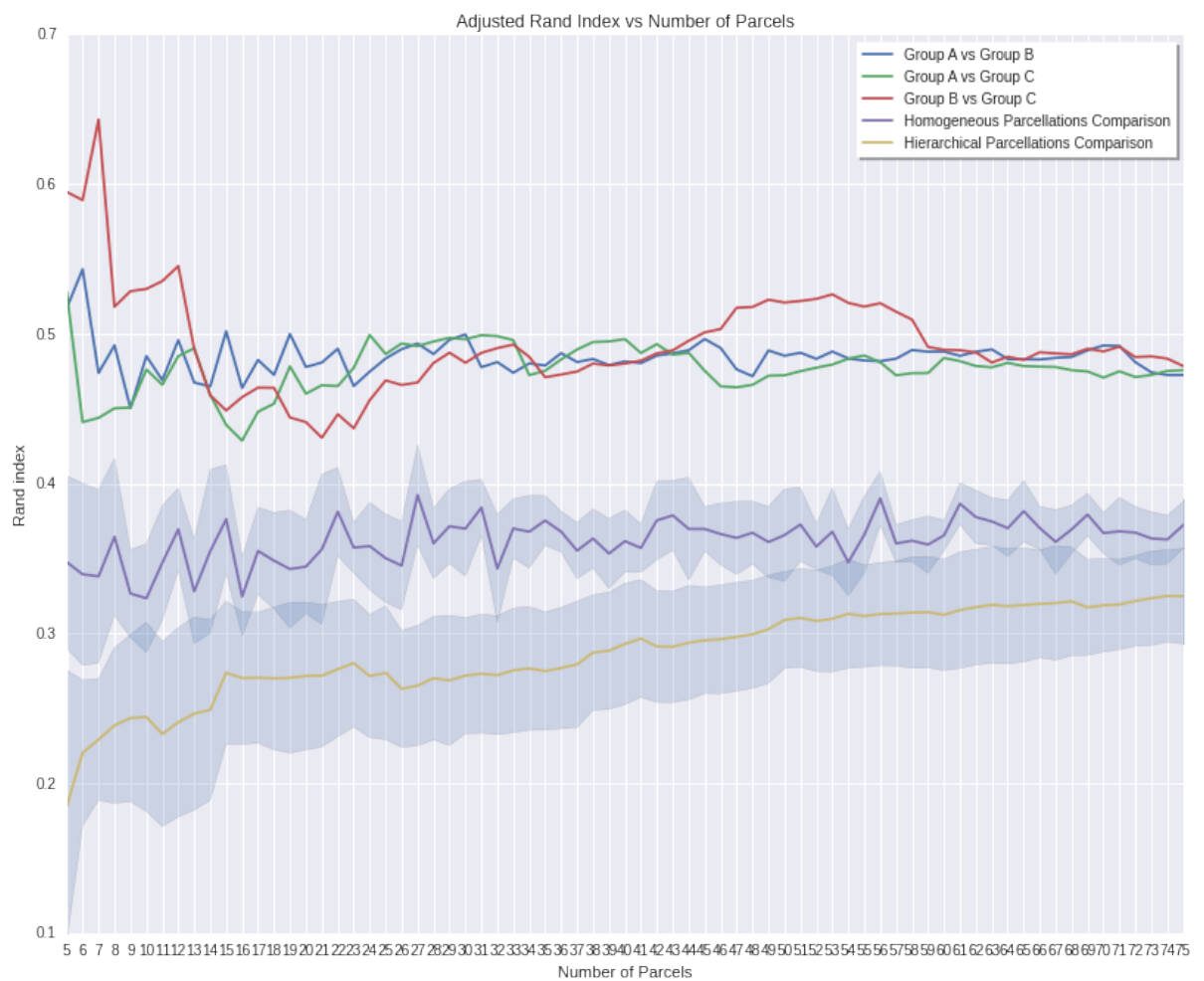


**Figure 5.5:** Adjusted Rand Index obtained when comparing: (red) Group A vs Group B; (blue) Group A vs Group C; (green) Group B vs Group C; (purple) Synthetic Homogeneous Parcels and (yellow) Synthetic hierarchical Parcels.

## 5. GROUPWISE STRUCTURAL PARCELLATION OF THE WHOLE CORTEX: A LOGISTIC RANDOM EFFECTS MODEL BASED APPROACH

---

**Table 1. Correlation value reported (Neurosynth)**

Parcel	Term	<i>r</i> (Thiebaut et al.)	<i>r</i> (Ours)
<b>1</b>	foot	0.267	<b>0.319</b>
<b>2</b>	motor	0.129	<b>0.208</b>
<b>3</b>	eye field	0.081	0.048
<b>4</b>	speech production	0.077	<b>0.138</b>
<b>5</b>	pre sma	0.245	0.234
<b>6</b>	phonological	0.206	0.019
<b>7</b>	-	-	-
<b>8</b>	executive control	0.049	0.042
<b>9</b>	-	-	-
<b>10</b>	semantic	0.178	<b>0.226</b>
<b>11</b>	social	0.137	0.110
<b>12</b>	semantic	0.139	0.086

Table 1. Spatial correlation value reported by Neurosynth for specific terms in each parcel of (**author?**)<sup>3</sup> and for our parcels. Enumeration comes from figure 5.6.

tion showed consistency with the one obtained by clustering only the tractograms in the frontal lobe. More specifically, the adjusted Rand index score between them was 0.65. We repeated this procedure for the 3 disjoins groups from the previous experiment. In each group, both frontal lobe parcellations showed to be consistent, achieving an adjusted Rand index of  $0.57 \pm 0.04$ .

our parcels and then calculated: how many of our parcels were contained by a anatomical region in more than a 90%, and which anatomical regions were contained inside of one of our parcels. Using this criterion, the Insula; Cingulate; Lateral-Occipital; Fusiform; Superior Frontal; Lingual; Sensory and Motor Cortex appear to be found as shown in Fig. 5.8.

### Anatomical Relationship of Our Parcels and Functional

### Functional Specialization.

Here we present a proof of concept that our technique creates parcels within anatomical boundaries and with functional meaning. To do so, first, we extracted a parcellation with 55 parcels from the groupwise parcellation computed from the 138 subjects. This was made to get a parcellation with coarse granularity while having at least the amount of parcels in the anatomical atlas of Desikan<sup>17</sup> (36 parcels). We compare this extracted parcellation against the Desikan Atlas and a functional study made to every subject in the HCP<sup>18</sup>.

### Relationship with Anatomical Boundaries

To assess if some anatomical structures were present in the dendrogram and if our resulting parcels were subdividing them, we compared our extracted parcellation with the Desikan atlas<sup>17</sup>. To do so, we projected the Desikan regions over

To study the relationship between our parcels and brain function, we projected our parcels over z-score maps representing responses to functional stimuli<sup>25</sup>. These maps are available as part of the HCP data, and represent the average activation of 100 subjects. In particular, we used the maps related to the following tasks: right hand, foot and tongue movement; face, shape recognition and story categorization. For information on the functional tasks, acquisition and processing of this data please refer to (**author?**)<sup>25</sup>. Figure 5.9 shows our parcels projected over contrasts in motor tasks. In particular, our parcels are projected over the following contrasts: tongue-average; hand movement-average and foot movement-average. Figure 5.10 shows our parcels projected over contrasts in cognitive tasks: face-shape recognition; shape-face recognition and short-story categorization. The figures show a good overlap between our parcels and the

## 5. GROUPWISE STRUCTURAL PARCELLATION OF THE WHOLE CORTEX: A LOGISTIC RANDOM EFFECTS MODEL BASED APPROACH

---

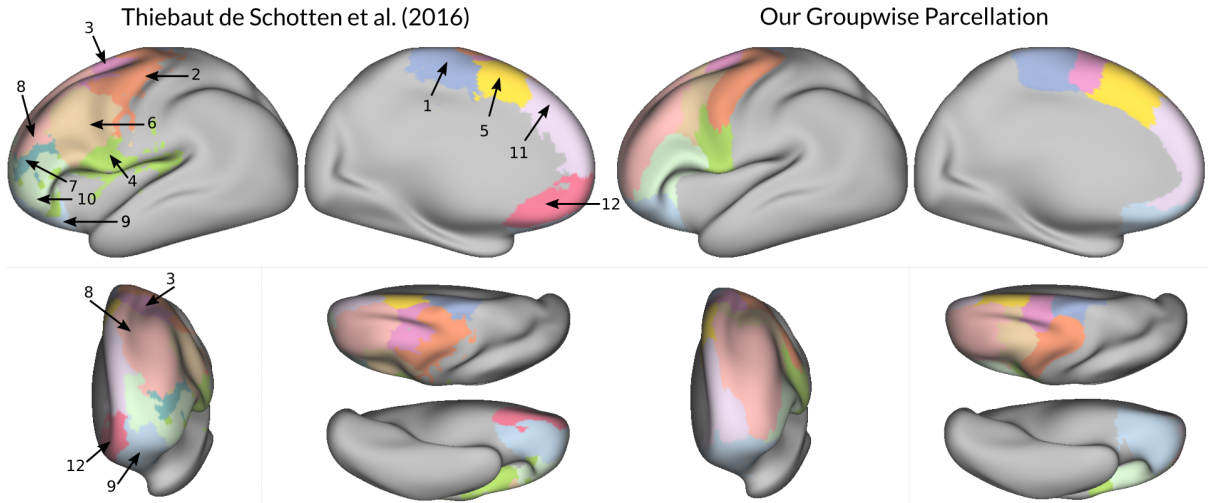


**Figure 5.6:** (author?)<sup>3</sup> parcellation (left) and our groupwise parcellation using only tractograms from the frontal lobe (right). Our parcels are colored after the parcel from (author?)<sup>3</sup> with which they best overlap.

regions with maximum activation of each task. In both figures the distribution of z-scores inside of specific regions are shown as histograms. Further information about the z-score is present in tables 2 and 3. These tables show that our parcels contain zero or few negative values; that the mean of their contained z-score is always positive and also, that many of those parcels enclose the maximum achievable z-score.

### Relationship with a Multi-Modal Parcellation of the Cortex

Finally, we study the (dis)similarities between our groupwise parcellation and that of (author?)<sup>19</sup>. In their work, (author?)<sup>19</sup> compute a parcellation of the whole cortex using information from different MRI modalities. In particular, they use information from task functional MRI; resting state functional MRI; myelin maps computed from T1 and T2 images and cortical thickness. It is important to remark that dMRI data, in which our work is solely based, was not used to construct their parcellation.

To compare our results against Glasser's atlas, we first extracted a parcellation of 180 parcels from the groupwise dendrogram of our 138 HCP subjects. That is, we extracted a parcellation with the same number of parcels as Glasser's one. Figure 5.11 show both parcellations side by side. We compared

both parcellations using the adjusted Rand Index, obtaining a score of 0.28. Such low score indicates that there's almost no similarity between our result and that of (author?)<sup>19</sup>. Also, there's no relationship with our groupwise parcellation with 55 parcels used in the previous section since Glasser's parcels (finest) do not subdivide ours (coarsest). Since Glasser's parcellation comes from functional information in the HCP, we studied the functional specialization of its parcels in the same manner as previous section. Figure 5.12 shows the histogram of z-score contained for some parcels when using the same maps as in section Functional Activations. It's important to remark that the z-score maps used come from responses to functional stimuli of HCP subjects<sup>18</sup>. In particular, histograms a; b and c in fig. 5.12 show that their subdivisions of the sensori-motor cortex contain a wide range of z-scores, centered in zero.

## 5.5. Discussion

---

In this work we presented a parsimonious statistical model for long-ranged axonal connectivity. Our model (section 5.3.1), assumes that the cortex is divided in patches of homogeneous extrinsic connectivity, as histological results showed in the macaque brain<sup>4</sup>. By borrowing ideas from statistical clustered data models<sup>15</sup>, our model accounts

## 5. GROUPWISE STRUCTURAL PARCELLATION OF THE WHOLE CORTEX: A LOGISTIC RANDOM EFFECTS MODEL BASED APPROACH

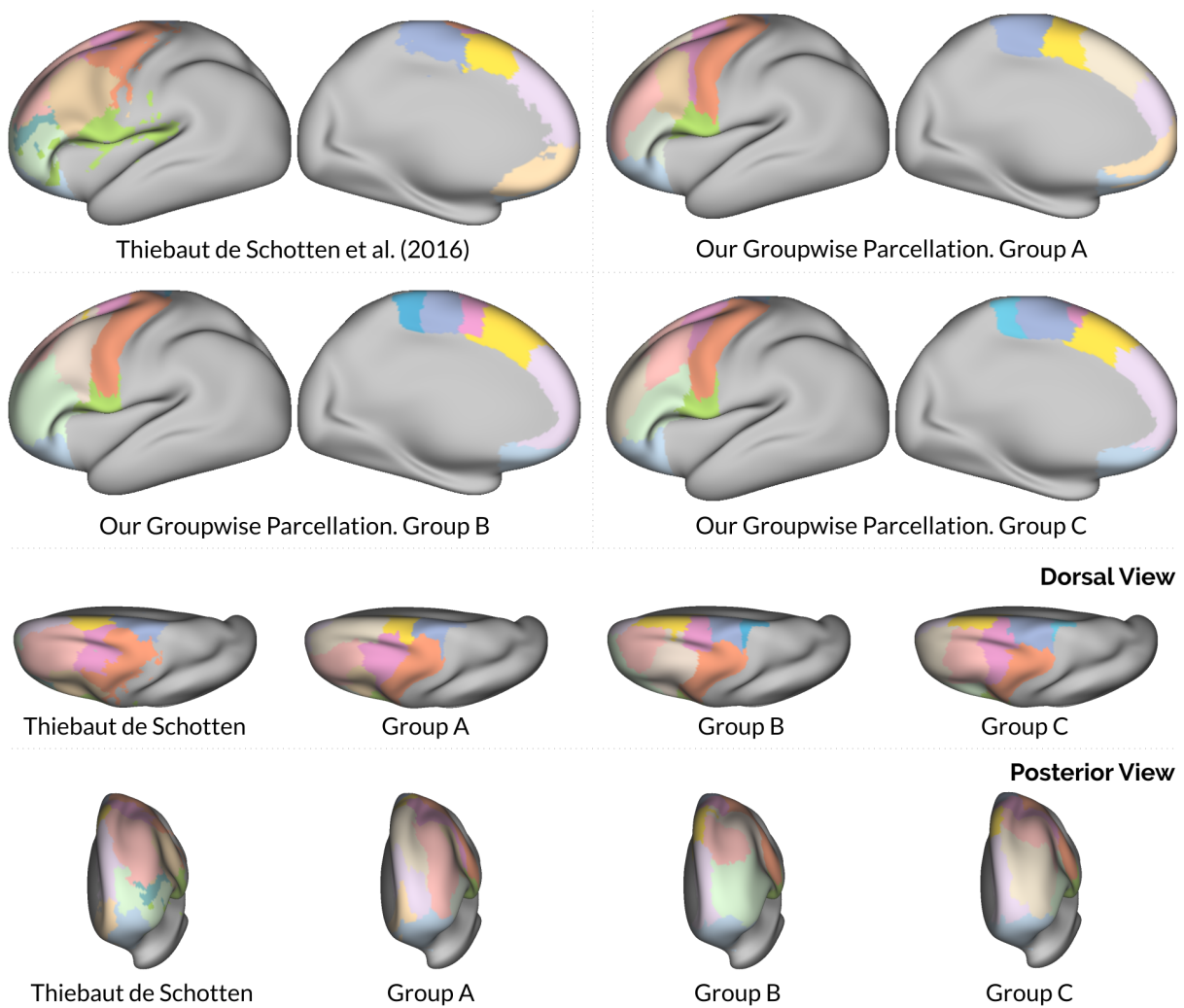


**Figure 5.7:** (author?)<sup>3</sup> parcellation (top-left) and our frontal lobe groupwise parcellations computed over 3 disjoint groups of subjects. Our parcels are colored after the parcel from (author?)<sup>3</sup> with which they best overlap.

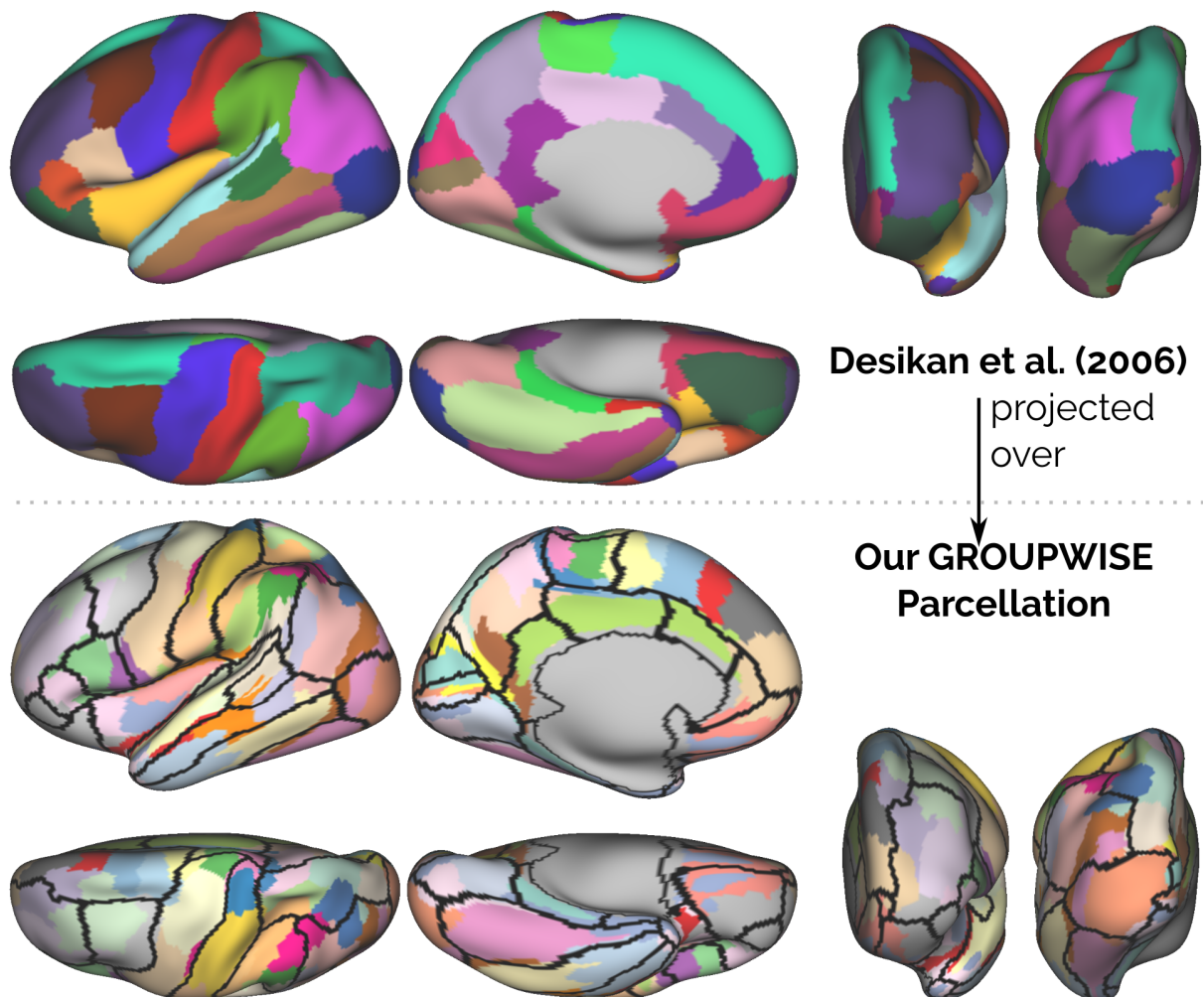


**Figure 5.8:** Relation between our pure extrinsic parcellation and the anatomical atlas of Desikan<sup>17</sup>. Desikan atlas projected over the groupwise parcellation with 55 parcels. Insula; Cingulate; Lateral-Occipital; Fusiform; Superior Frontal; Lingual; Sensory and Motor Cortex appear to be found.

5. GROUPWISE STRUCTURAL PARCELLATION OF THE WHOLE CORTEX: A LOGISTIC RANDOM EFFECTS MODEL BASED APPROACH

---

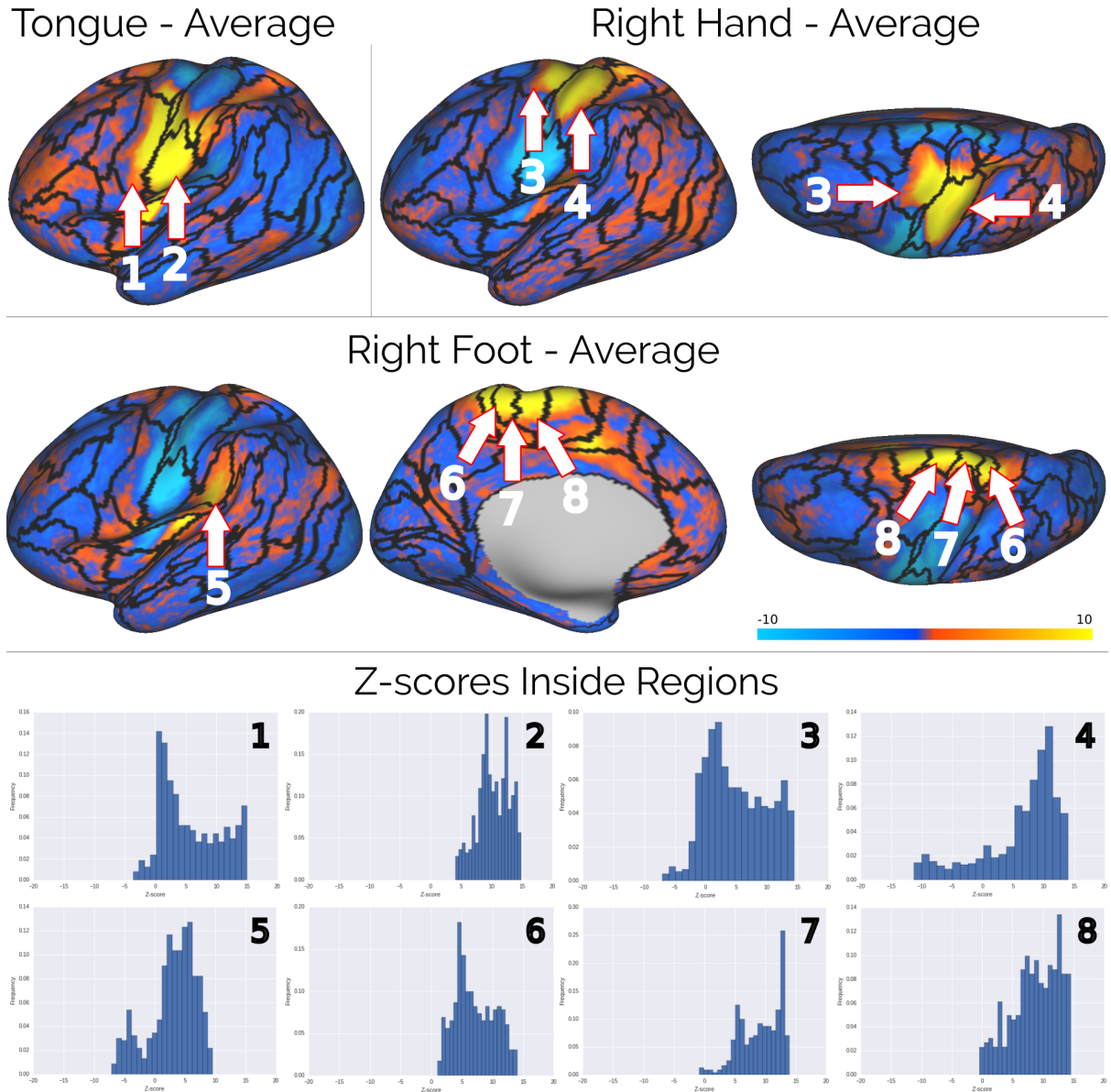


**Figure 5.9:** Our groupwise parcellation with 55 parcels projected over z-scores representing responses to motor tasks. Each histogram shows the distribution of z-score inside our parcels. The null or small fraction of negative values shows the functional specialization of our parcels

5. GROUPWISE STRUCTURAL PARCELLATION OF THE WHOLE CORTEX: A LOGISTIC RANDOM EFFECTS MODEL BASED APPROACH

---

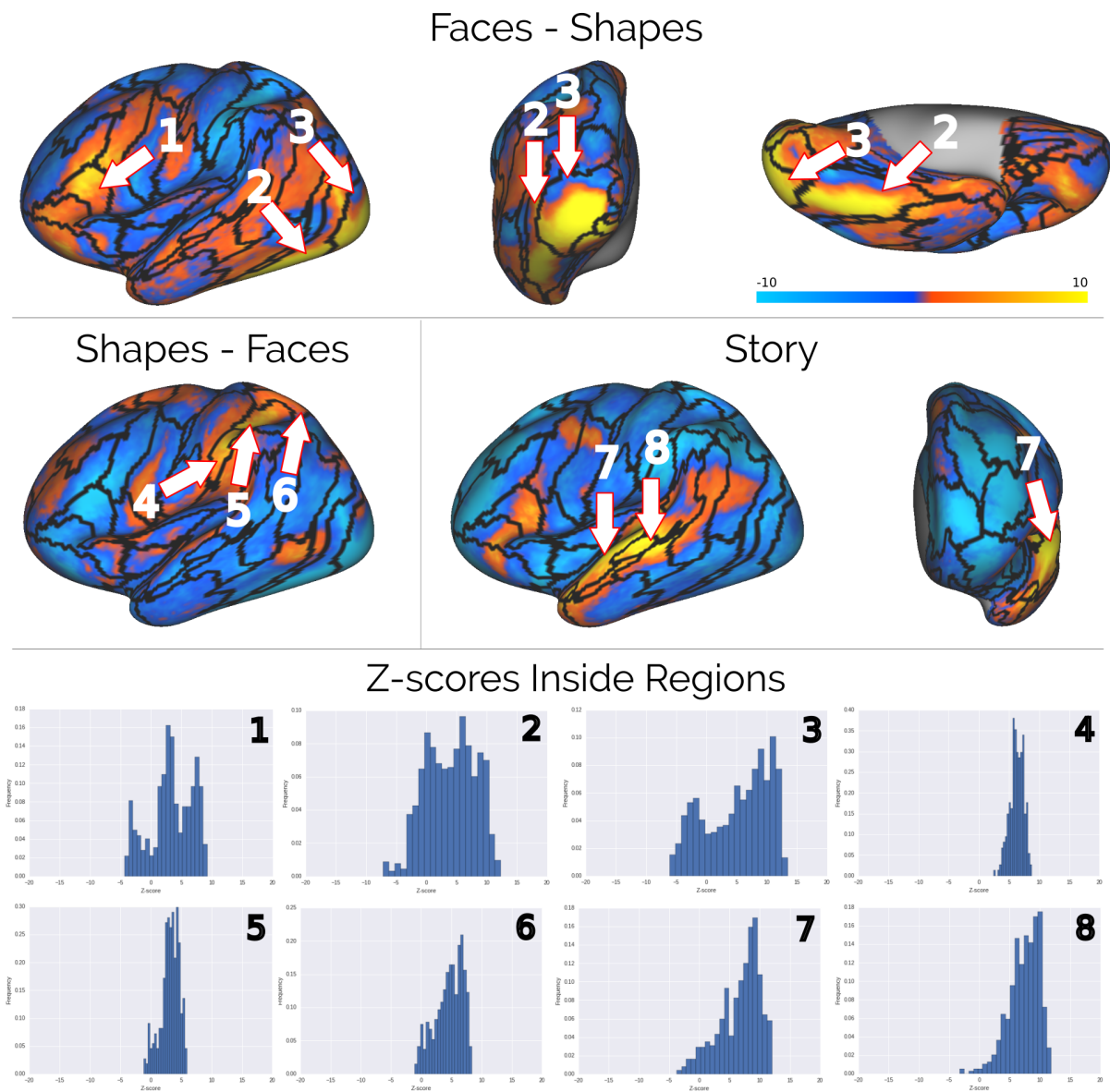


**Figure 5.10:** Our groupwise parcellation with 55 parcels projected over z-scores representing responses to cognitive tasks. Each histogram shows the distribution of z-score inside our parcels. The null or small fraction of negative values shows the functional specialization of our parcels

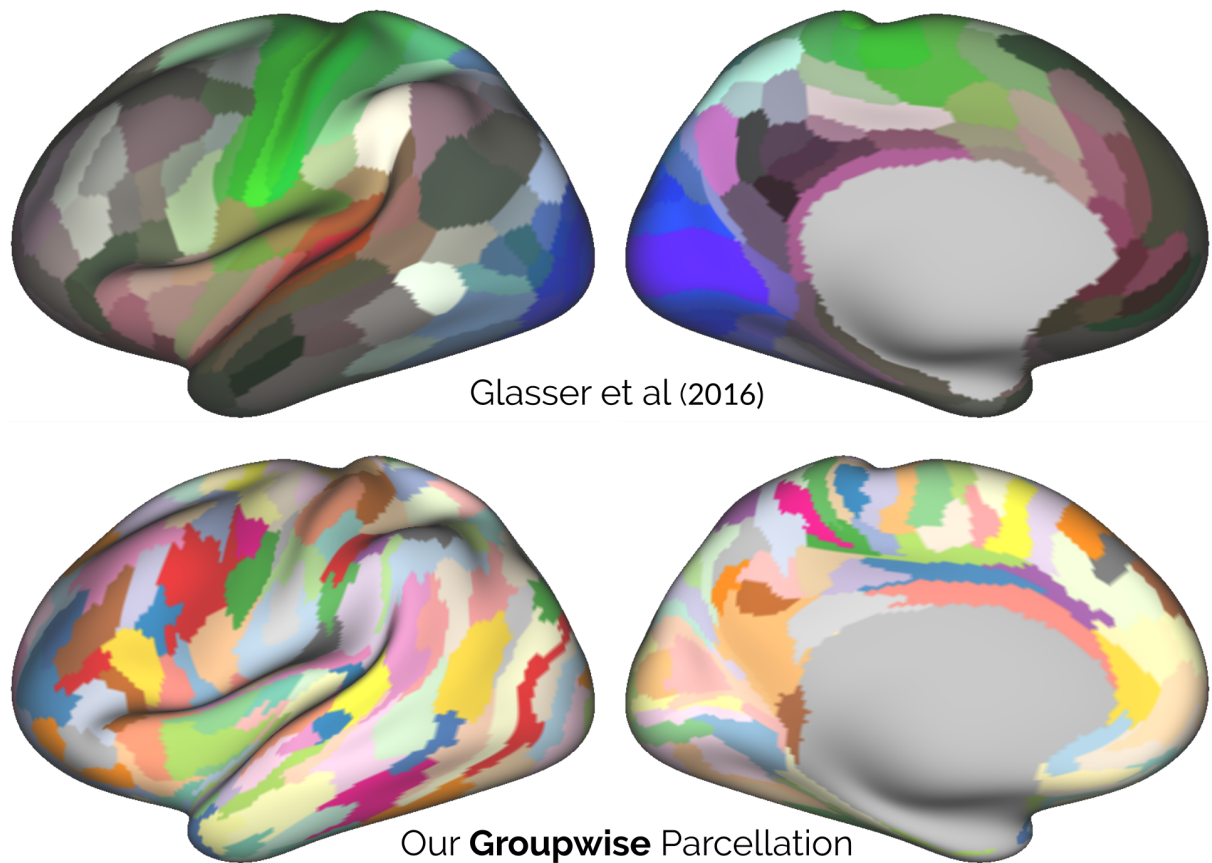


**Figure 5.11:** (author?)<sup>19</sup> parcellation (upper) and our groupwise parcellations computed from 138 HCP subjects. Both parcellations contain 180 parcels. There's almost no overlap according to the adjusted Rand index between them (0.28).

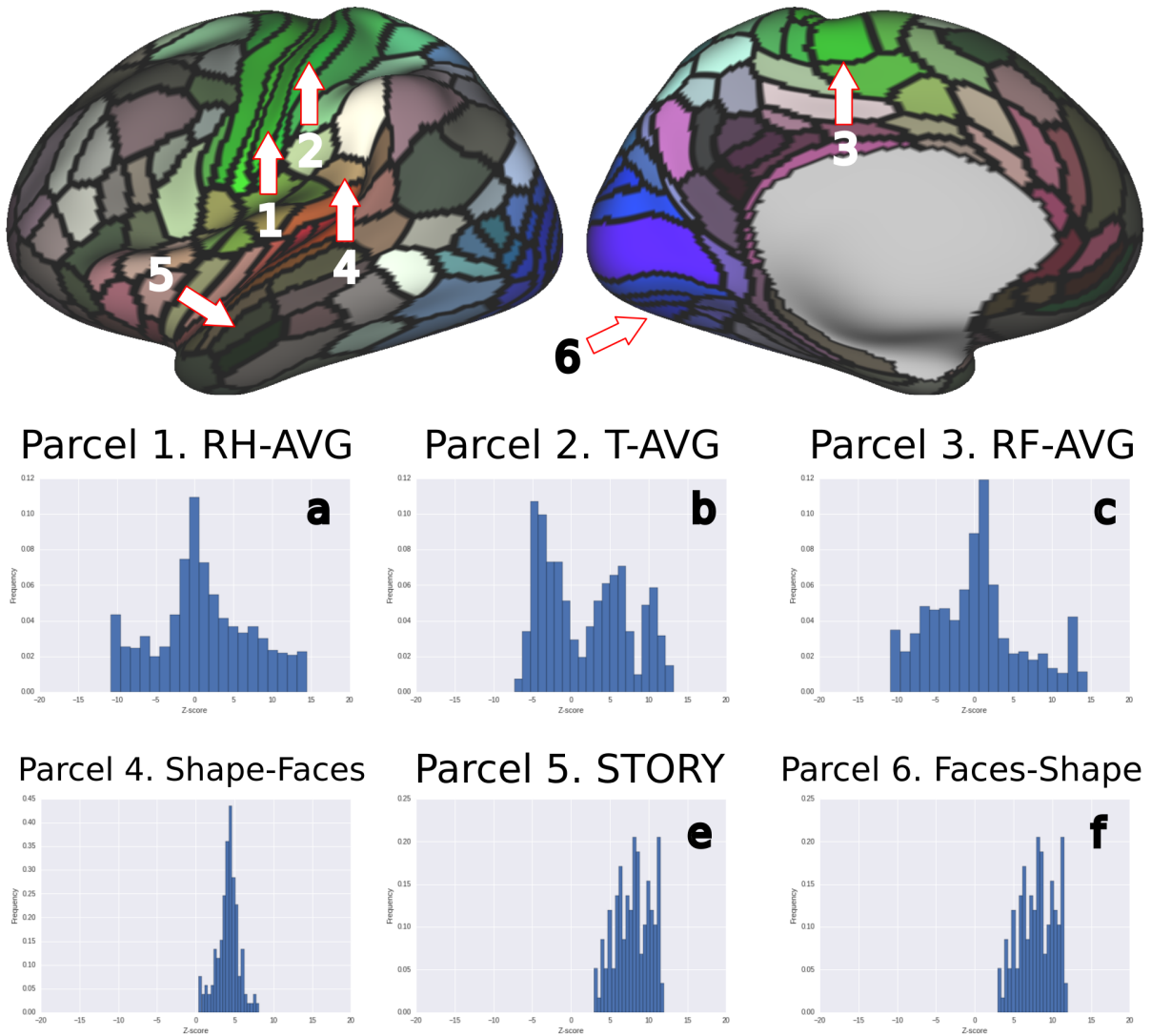


**Figure 5.12:** (author?)<sup>19</sup> parcellation (upper) and histograms of z-score contained in different parcels for different functional task. (a) Histogram for parcel 1 for the contrast related to Tongue movement. (b) Histogram for parcel 2 for the contrast related to Tongue movement. (c) Histogram for parcel 3 for the contrast related to Right Foot movement. (d) Histogram for parcel 4 for the contrast Shape recognition vs Face recognition. (e) Histogram for parcel 5 for the contrast related to Story Categorization. (f) Histogram for parcel 5 for the contrast Face recognition vs Shape recognition. The histograms (d); (e) and (f) correspond to the parcels with the greatest mean z-score of their respective tasks.

## 5. GROUPWISE STRUCTURAL PARCELLATION OF THE WHOLE CORTEX: A LOGISTIC RANDOM EFFECTS MODEL BASED APPROACH

---

**Table 2. Statistics on z-score distribution in parcels from figure 5.9**

Contrast	Parcel	Min.	Max.	Mean ± Std. Dev.	Max. Score in Map
T-Avg	<b>1</b>	-3.62	15.03	5.67±4.91	15.03
T-Avg	<b>2</b>	4.11	14.88	10.30 ± 2.56	15.03
RH-Avg	<b>3</b>	-7.02	14.50	5.05 ± 4.95	14.50
RH-Avg	<b>4</b>	-11.25	14.07	6.35 ± 6.25	14.50
RF-Avg	<b>5</b>	-7.10	9.57	2.99 ± 3.84	14.56
RF-Avg	<b>6</b>	1.04	14.01	7.13 ± 3.20	14.56
RF-Avg	<b>7</b>	-0.83	13.98	9.23 ± 3.32	14.56
RF-Avg	<b>8</b>	-0.46	14.56	8.73 ± 3.81	14.56

---

Table 2. Minimum; maximum and mean z-score contained by each of the parcels enumerated in figure 5.9. The highest z-score of each map is reported to facilitate comparison. T-Avg: Tongue movement versus average; RH-Avg: Right Hand Movement versus average; RF-Avg: Right Foot Movement versus average.

**Table 3. Statistics on z-score distribution in parcels from figure 5.10**

Contrast	Parcel	Min.	Max.	Mean ± Std. Dev.	Max. Score in map
Faces-Shapes	<b>1</b>	-4.33	9.28	3.35 ± 3.51	13.45
Faces-Shapes	<b>2</b>	-7.16	12.36	4.01 ± 4.09	13.45
Faces-Shapes	<b>3</b>	-6.07	13.45	5.16 ± 5.25	13.45
Shapes-Faces	<b>4</b>	-5.73	5.37	0.93 ± 1.78	8.79
Shapes-Faces	<b>5</b>	-4.11	7.67	1.11 ± 2.11	8.79
Shapes-Faces	<b>6</b>	-1.13	5.94	3.17 ± 1.49	8.79
Story	<b>7</b>	-3.72	12.02	6.72 ± 3.35	12.02
Story	<b>8</b>	-3.24	11.92	7.41 ± 2.50	12.02

---

Table 3. Minimum; maximum and mean z-score contained by each of the parcels enumerated in figure 5.10. The highest z-score of each map is reported to facilitate comparison. Faces-Shapes: Face recognition versus shape recognition contrast; Shapes-Faces: Shape recognition versus face recognition; Story: Short story categorization.

for the variability in the axonal connections of a patch's neurons and for variability in patch boundaries across subjects.

Taking advantage of our proposed model, in Section 5.3.2 we presented an efficient technique to parcellate the cortex based on its extrinsic connectivity. Our technique uses only dMRI information, without the need of relying on initial parcellations<sup>8</sup>. Also, our technique allows parcellation of the whole cortex, overcoming the problem of working with only part of it<sup>9;10;11;3</sup>. Additionally, our technique allows creation of both single subject and groupwise parcellations. Our groupwise parcellation technique relies on anatomical seed-correspondence across subjects. In our experiments, this is achieved as each HCP subject possess a coregistered dense mesh representing they cortical surface<sup>18</sup>. Given the anatomical differences across-subjects, this purely anatomical matching of

seeds is probably sub-optimal. However, it allows us to compute single and groupwise parcellations independently. By doing this, we avoid the need to impose constraints between our single and group parcellations<sup>8;13;14</sup>.

Inspired by (**author?**)<sup>12</sup>, our technique uses Hierarchical Clustering to comprise multiple granularities of the same parcellation in a dendrogram. This allows us to overcome the need of other techniques<sup>14</sup> to specify an expected number of clusters. Hence, we dont need to recompute the whole pipeline each time a new parcellation is required. As in (**author?**)<sup>12</sup>, we also create the dendrogram using only one comprehensive parameter: the minimum size of each cluster. This parameter imposes the local coherence criterion. Our fundamental difference with Moreno-Dominguez' technique is how we compare and merge tractograms during the clustering process. (**author?**)<sup>12</sup> use Centroid Cluster-

## 5. GROUPWISE STRUCTURAL PARCELLATION OF THE WHOLE CORTEX: A LOGISTIC RANDOM EFFECTS MODEL BASED APPROACH

---

ing<sup>33</sup> with the cosine distance. This can lead to an erroneous parcellation since the centroid criterion doesn't minimize the cosine distance between points. Also, their method creates dendograms with inversions<sup>33</sup>, which are then removed heuristically. In our case, using a Logistic Random Effect model (eq. 5.5) allowed us to transform the tractograms into a Euclidean space (sec. 5.3.2) and compare them using the Euclidean distance. In doing this, it is important to remark that we are making a trade off. Since we are comparing high-dimensional vectors with the Euclidean distance, we are probably affected by the dimensionality curse<sup>34</sup>. However, working in an Euclidean space possess many advantages. The first advantage is that we can compute clusters with minimum intra-cluster variance by using Ward's Hierarchical method. We can use this algorithm since its only hypothesis is that the features to cluster are in a Euclidean space. Also, since we work with the Euclidean distance, we can apply the Lance and Williams<sup>35</sup> formula during clustering. This formula gives us the dissimilarity between the new centroid created at each step and the rest of the existing tractograms in constant time. As far as we know there's no Lance and Williams formula when using the cosine distance with the centroid linkage. This allows us to lower the time complexity of our algorithm with respect to Moreno-Dominguez. Since we use Ward's clustering, our resulting dendograms do not have inversions, which means that we don't need to post-process them. Another advantage is that we can retrieve a parcellation from the dendrogram using a simple technique: horizontal cut<sup>29</sup>. While other methods to cut the dendrogram exist<sup>29</sup>, horizontal cut is sufficient to solve our Gaussian Mixture Model (eq. 5.5) as shown in ?. Finally, even if our algorithm is probably affected by the dimensionality curse, our parcellations showed to be consistent across-groups and in agreement with extant parcellations in the literature.

### Across Groupwise Parcellations are Consistent

We assessed the consistency of our groupwise parcellation by quantifying the consistency across 3 disjoint groups of 46 subjects each. The consistency is shown by the adjusted Rand index in

Fig. 5.5, which quantifies consistency across parcellations<sup>30</sup>. As seen in Fig. 5.5 whole-cortex parcellations obtained with our method are consistent across groups, and the Adjusted Rand Index is significantly higher, i.e. more than 3 standard deviations, for all granularities when compared with the null case of randomly-generated parcellations.

Our whole-cortex groupwise parcellation reaches a maximum consistency score when the cortex is divided in 6 regions, see Fig. 5.5. As seen in Fig. 5.3, these parcellations are consistent with specific anatomo/functional networks: the frontal lobe section anterior to the prefrontal cortex is shown in yellow; the sensorimotor area is shown in cyan, the cingulate area is shown in beige; the fronto-occipital connection in orange, and the temporo-parietal system in pink.

### Our Method Create Parcels in Agreement with Extant in the Literature.

We showed that our technique obtains results similar to another method extant in the literature. We did so by parceling only the frontal and showing the visual similarity between our resulting parcels and those obtained by (**author?**)<sup>3</sup>. Moreover, the blue, pink and green parcels in fig. 5.6 share not only similar boundaries and location, but also functional specialization (Table 1). In some cases our parcels possess even higher spatial-correlation with functional task according to Neurosynth's<sup>16</sup> Decode tool<sup>4</sup>. We assessed the consistency of our obtained groupwise parcellation by computing the groupwise frontal lobe parcellation of three disjoints groups of 46 subjects and comparing them using the adjusted Rand index. The obtained value of 0.61 shows that our parcellation of the frontal lobe is consistent across groups.

### Our Method with Brain Anatomy. Parcels in

We showed that many of our parcels are in agreement with brain anatomy. In particular, we showed that in our groupwise parcellation, with 55 parcels, the following anatomical structures appeared to be found: Cingulate; Insula; Lateral-Occipital;

<sup>4</sup><http://neurosynth.org/decode/>

## 5. GROUPWISE STRUCTURAL PARCELLATION OF THE WHOLE CORTEX: A LOGISTIC RANDOM EFFECTS MODEL BASED APPROACH

---

Fusiform; Superior Frontal; Lingual; Motor and Sensory cortex. Here we discuss why some of these parcels were found and how are their connectivity fingerprints. In the case of the Cingulate, its fingerprint, shown in fig. 5.13, is strongly related with the Cingulate Fascicle (CF) pathway. This is consistent with the fact that the seeds located in the Cingulate will end up into the CF after being pushed in the white-matter. In the case of the Insula, each subdivision showed a specific pattern of connectivity as shown in fig. 5.13. These parcels show a gradient of connections from the occipital lobe to the frontal lobe consistent with that of (author?)<sup>36</sup>. In the Lateral-Occipital region, we see a specific pattern of local connectivity which cannot be attributed to gyral bias since the Lateral-Occipital covers many sulci and gyrus. In the case of the fusiform, it is almost completely contained in one of our parcellations, which goes from the Fusiform up to the Lateral-Occipital (fig. 5.8). This could add evidence to the hypothesis that the Fusiform plays a role in visual tasks<sup>37;38</sup>. Finally, the Motor and Sensory cortex appear to be found. While the appearance of each gyri is most probably because of gyral bias<sup>6</sup>, the parcels inside them show specific patterns of structural connectivity (fig. 5.13), and, as seen in section 3.5.2, functional specialization.

### Our Results Show a Closest Relationship Between Structural Connectivity and Brain Function.

We assessed the functional specialization of some of our parcels by showing how they overlap with responses to functional and cognitive tasks measured with fMRI. In particular, for all the studied tasks, the parcels contained a higher proportion of positive values than negative ones as expressed by the positive mean values reported in tables 2 and 3. For some parcels there were not even negative values. Moreover, several of the histograms on figures 5.9 and 5.10 show a high frequency of z-score values greater than 5, which indicate a significant correlation with functional activation. Therefore, our results show, for some tasks, the strong relationship between extrinsic connectivity and functional specialization in the human brain cortex.

### Our Parcels Are Not Simpler Than Those Obtained By Glasser et al. (2016), But Possess Better Functional Specialization for Motor Tasks.

Our parcels were not related to those of (author?)<sup>19</sup>. This is shown by the obtained adjusted Rand index score between them (0.28). It's important to remark that our parcels are purely based on extrinsic connectivity, meanwhile those of (author?)<sup>19</sup> do not use dMRI information. Glasser's parcels are mostly based on myelin and functional information. In particular, their subdivision of the sensori-motor cortex (green parcels in fig. 5.11) is mostly based in Myelin maps as shown in Figure 4.a of (author?)<sup>19</sup>. Because of this, their parcels in the sensori-motor cortex contain a wide range of z-scores when compared with responses to functional stimuli as shown by histograms a; b and c in fig. 5.12. In contrast, our parcels in the sensori-motor cortex, for a coarser parcellation, show a good overlap with function and are in agreement with the motor strip mapping as discussed in the previous section. Also, for the case of story categorization; shape recognition and face recognition, our parcels show a similar distribution of z-scores (fig. 5.9) than those with the highest mean z-scores of (author?)<sup>19</sup> (parcels d; e and f of fig. 5.12).

## 5.6. Conclusion

---

Understanding how the brain is structurally organized and how it constraints functionality is an open question in neuroscience. Recent advances in acquisition and modeling techniques on dMRI have facilitated to study axonal connectivity in the brain. However, parcelling the whole cortex based on a structural criterion remained challenging. In this work we presented a connectivity model; framed tractography within our model and presented a parceling technique that allows parcelation of the whole brain in both single subject and groupwise cases. Our technique, along with the obtained groupwise parcellation, could have major implications both in cognitive neuroscience and in development-aging studies. At the same time, our technique could help to lower the gap between structural connectivity and brain function, since some of our pure structural parcels showed good overlapping with responses to functional tasks.

5. GROUPWISE STRUCTURAL PARCELLATION OF THE WHOLE CORTEX: A LOGISTIC RANDOM EFFECTS MODEL BASED APPROACH

---

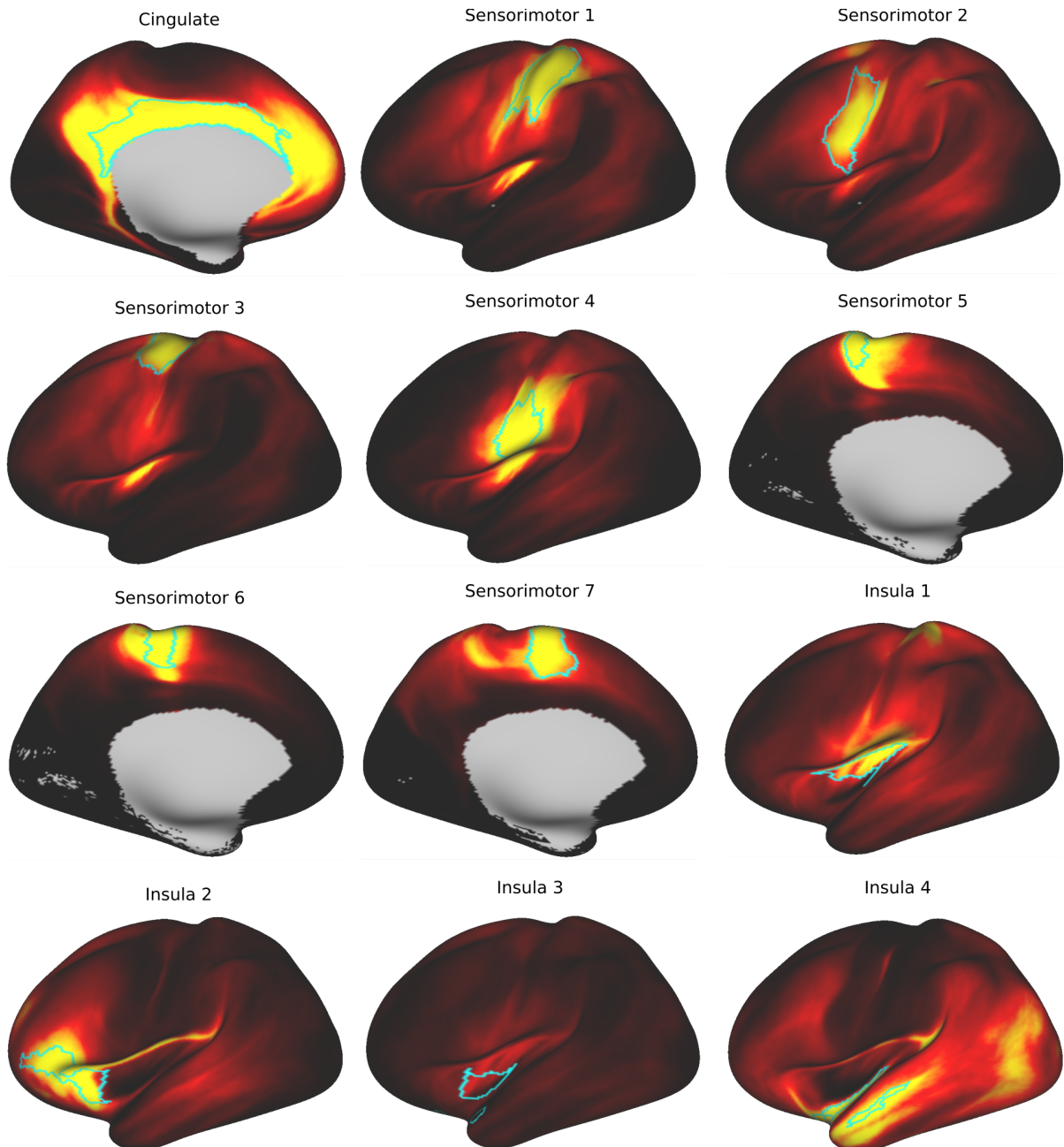


**Figure 5.13:** Connectivity fingerprint for different parcels in our groupwise parcellation. The names in the titles are given after the anatomical structure that they subdivide (or contain, as with the Fusiform).

## 5. GROUPWISE STRUCTURAL PARCELLATION OF THE WHOLE CORTEX: A LOGISTIC RANDOM EFFECTS MODEL BASED APPROACH

---

However, we still are left with the open question of how to match parcels across subjects. Even when our results show that our technique is stable across groups of subjects, at the single subject level is not easy to find correspondence between two parcellations. The following chapter of this thesis will work on this problem.

## Bibliography

---

- [1] K. Brodmann, *Vergleichende Lokalisationslehre der Großhirnrinde in ihren Prinzipien dargestellt auf Grund des Zellaufbaues*. Leipzig: Barth, 1909.
- [2] B. Thirion, G. Varoquaux, E. Dohmatob, and J. B. Poline, “Which fMRI clustering gives good brain parcellations?,” *Front. Neurosci.*, vol. 8, no. 8 JUL, pp. 1–13, 2014.
- [3] M. Thiebaut de Schotten, M. Urbanski, B. Ba-trancourt, R. Levy, B. Dubois, L. Cerliani, and E. Volle, “Rostro-caudal Architecture of the Frontal Lobes in Humans,” *Cereb. Cortex*, pp. 1–15, 2016.
- [4] J. D. Schmahmann and D. N. Pandya, *Fiber Pathways of the Brain*, vol. 1. Oxford University Press, apr 2006.
- [5] R. E. Passingham, K. E. Stephan, and R. Kötter, “The anatomical basis of functional localization in the cortex,” *Nat. Rev. Neurosci.*, vol. 3, pp. 606–616, aug 2002.
- [6] D. C. Van Essen, S. Jbabdi, S. N. Sotiroopoulos, C. Chen, K. Dikranian, T. Coalson, J. Harwell, T. E. Behrens, and M. F. Glasser, “Mapping Connections in Humans and Non-Human Primates,” in *Diffus. MRI*, no. January 2014, pp. 337–358, Elsevier, 2014.
- [7] S. Jbabdi and T. E. Behrens, “Long-range connectomics,” *Ann. N. Y. Acad. Sci.*, vol. 1305, pp. 83–93, dec 2013.
- [8] M. J. Clarkson, I. B. Malone, M. Modat, K. K. Leung, N. Ryan, D. C. Alexander, N. C. Fox, and S. Ourselin, *A Framework For Using Diffusion Weighted Imaging To Improve Cortical Parcellation*, vol. 6362 of *Lecture Notes in Computer Science*. Berlin, Heidelberg: Springer Berlin Heidelberg, 2010.
- [9] S. Lefranc, P. Roca, M. Perrot, C. Poupon, D. Le Bihan, J.-F. Mangin, and D. Rivière, “Groupwise connectivity-based parcellation of the whole human cortical surface using watershed-driven dimension reduction,” *Med. Image Anal.*, vol. 30, pp. 11–29, may 2016.
- [10] P. Roca, D. Rivière, P. Guevara, C. Poupon, and J. F. Mangin, “Tractography-based parcellation of the cortex using a spatially-informed dimension reduction of the connectivity matrix,” *Lect. Notes Comput. Sci. (including Subser. Lect. Notes Artif. Intell. Lect. Notes Bioinformatics)*, vol. 5761 LNCS, no. PART 1, pp. 935–942, 2009.
- [11] M. Thiebaut de Schotten, M. Urbanski, R. Valabregue, D. J. Bayle, and E. Volle, “Subdivision of the occipital lobes: An anatomical and functional MRI connectivity study,” *Cortex*, vol. 56, pp. 121–137, 2014.
- [12] D. Moreno-Dominguez, A. Anwander, and T. R. Knösche, “A hierarchical method for whole-brain connectivity-based parcellation,” *Hum. Brain Mapp.*, vol. 35, pp. 5000–5025, oct 2014.
- [13] P. Roca, A. Tucholka, D. Rivière, P. Guevara, C. Poupon, and J. F. Mangin, “Inter-subject connectivity-based parcellation of a patch of cerebral cortex,” *Lect. Notes Comput. Sci. (including Subser. Lect. Notes Artif. Intell. Lect. Notes Bioinformatics)*, vol. 6362 LNCS, no. PART 2, pp. 347–354, 2010.
- [14] S. Parisot, S. Arslan, J. Passerat-Palmbach, W. M. Wells, and D. Rueckert, “Tractography-Driven Groupwise Multi-scale Parcellation of the Cortex.,” *Inf. Process. Med. Imaging*, vol. 24, pp. 600–12, 2015.
- [15] J. F. Pendergast, S. J. Gange, M. A. Newton, M. J. Lindstrom, M. Palta, and M. R. Fisher, “A Survey of Methods for Analyzing Clustered Binary Response Data,” *Int. Stat. Rev. / Rev. Int. Stat.*, vol. 64, p. 89, apr 1996.
- [16] T. Yarkoni, R. A. Poldrack, T. E. Nichols, D. C. Van Essen, and T. D. Wager,

## 5. GROUPWISE STRUCTURAL PARCELLATION OF THE WHOLE CORTEX: A LOGISTIC RANDOM EFFECTS MODEL BASED APPROACH

---

- “Large-scale automated synthesis of human functional neuroimaging data,” *Nat. Methods*, vol. 8, pp. 665–670, jun 2011.
- [17] R. S. Desikan, F. Ségonne, B. Fischl, B. T. Quinn, B. C. Dickerson, D. Blacker, R. L. Buckner, A. M. Dale, R. P. Maguire, B. T. Hyman, M. S. Albert, and R. J. Killiany, “An automated labeling system for subdividing the human cerebral cortex on MRI scans into gyral based regions of interest,” *Neuroimage*, vol. 31, pp. 968–980, jul 2006.
  - [18] M. F. Glasser, S. N. Sotiroopoulos, J. A. Wilson, T. S. Coalson, B. Fischl, J. L. Andersson, J. Xu, S. Jbabdi, M. Webster, J. R. Polimeni, D. C. Van Essen, and M. Jenkinson, “The minimal preprocessing pipelines for the Human Connectome Project,” *Neuroimage*, vol. 80, pp. 105–124, oct 2013.
  - [19] M. F. Glasser, T. S. Coalson, E. C. Robinson, C. D. Hacker, J. Harwell, E. Yacoub, K. Ugurbil, J. Andersson, C. F. Beckmann, M. Jenkinson, S. M. Smith, and D. C. Van Essen, “A multi-modal parcellation of human cerebral cortex.,” *Nature*, vol. 536, no. 7615, pp. 171–8, 2016.
  - [20] T. Behrens, M. Woolrich, M. Jenkinson, H. Johansen-Berg, R. Nunes, S. Clare, P. Matthews, J. Brady, and S. Smith, “Characterization and propagation of uncertainty in diffusion-weighted MR imaging,” *Magn. Reson. Med.*, vol. 50, pp. 1077–1088, nov 2003.
  - [21] J. A. N. McCullagh, P., *Generalized Linear Models*. London: Chapman and Hall/CRC, 2 ed., 1989.
  - [22] K. M. Pohl, J. Fisher, S. Bouix, M. Shenton, R. W. McCarley, W. E. L. Grimson, R. Kikinis, and W. M. Wells, “Using the logarithm of odds to define a vector space on probabilistic atlases,” *Med. Image Anal.*, vol. 11, pp. 465–477, oct 2007.
  - [23] J. Ward Jr., “Hierarchical Grouping to Optimize an Objective Function,” *J. Am. Stat. Assoc.*, vol. 58, no. 301, pp. 236–244, 1963.
  - [24] D. C. Van Essen, K. Ugurbil, E. Auerbach, D. Barch, T. E. J. Behrens, R. Bucholz, A. Chang, L. Chen, M. Corbetta, S. W. Curtiss, S. Della Penna, D. Feinberg, M. F. Glasser, N. Harel, a. C. Heath, L. Larson-Prior, D. Marcus, G. Michalareas, S. Moeller, R. Oostenveld, S. E. Petersen, F. Prior, B. L. Schlaggar, S. M. Smith, a. Z. Snyder, J. Xu, and E. Yacoub, “The Human Connectome Project: A data acquisition perspective,” *Neuroimage*, vol. 62, no. 4, pp. 2222–2231, 2012.
  - [25] D. M. Barch, G. C. Burgess, M. P. Harms, S. E. Petersen, B. L. Schlaggar, M. Corbetta, M. F. Glasser, S. Curtiss, S. Dixit, C. Feldt, D. Nolan, E. Bryant, T. Hartley, O. Footer, J. M. Bjork, R. Poldrack, S. Smith, H. Johansen-Berg, A. Z. Snyder, and D. C. Van Essen, “Function in the human connectome: Task-fMRI and individual differences in behavior,” *Neuroimage*, vol. 80, pp. 169–189, oct 2013.
  - [26] J.-D. Tournier, F. Calamante, D. G. Gadian, and A. Connelly, “Direct estimation of the fiber orientation density function from diffusion-weighted MRI data using spherical deconvolution,” *Neuroimage*, vol. 23, pp. 1176–1185, nov 2004.
  - [27] C. Reveley, A. K. Seth, C. Pierpaoli, A. C. Silva, D. Yu, R. C. Saunders, D. a. Leopold, and F. Q. Ye, “Superficial white matter fiber systems impede detection of long-range cortical connections in diffusion MR tractography,” *Proc. Natl. Acad. Sci.*, vol. 112, pp. E2820–E2828, may 2015.
  - [28] E. Garyfallidis, M. Brett, B. Amirbekian, A. Rokem, S. van der Walt, M. Descoteaux, and I. Nimmo-Smith, “Dipy, a library for the analysis of diffusion MRI data,” *Front. Neuroinform.*, vol. 8, p. 8, feb 2014.
  - [29] F. Murtagh and P. Contreras, “Methods of Hierarchical Clustering,” *Empir. Econ.*, vol. 38, pp. 23–45, apr 2011.
  - [30] L. Hubert and P. Arabie, “Comparing partitions,” *J. Classif.*, vol. 2, pp. 193–218, dec 1985.

## 5. GROUPWISE STRUCTURAL PARCELLATION OF THE WHOLE CORTEX: A LOGISTIC RANDOM EFFECTS MODEL BASED APPROACH

---

- [31] K. J. Gorgolewski, G. Varoquaux, G. Rivera, Y. Schwartz, V. V. Sochat, S. S. Ghosh, C. Maumet, T. E. Nichols, J. B. Poline, T. Yarkoni, D. S. Margulies, and R. A. Poldrack, “NeuroVault.org: A repository for sharing unthresholded statistical maps, parcellations, and atlases of the human brain,” *Neuroimage*, vol. 124, no. April, pp. 1242–1244, 2016.
- [32] C. J. Holmes, R. Hoge, L. Collins, and A. C. Evans, “Enhancement of T1 MR images using registration for signal averaging,” *Neuroimage*, vol. 3, p. S28, jun 1996.
- [33] F. Murtagh, *Multidimensional Clustering Algorithms*. Vienna: Comps Physica Verlag, 1985.
- [34] K. Beyer, J. Goldstein, R. Ramakrishnan, and U. Shaft, “When is nearest neighbor meaningful?,” *Database TheoryICDT’99*, pp. 217–235, 1999.
- [35] B. G. N. Lance and W. T. Williams, “A general theory of classificatory sorting strategies 1 . Hierarchical systems,” *Comput. J.*, vol. 9, no. 4, pp. 373–380, 1967.
- [36] J. Ghaziri, A. Tucholka, G. Girard, J.-C. Houde, O. Boucher, G. Gilbert, M. Descoateaux, S. Lippe, P. Rainville, and D. K. Nguyen, “The Corticocortical Structural Connectivity of the Human Insula,” *Cereb Cortex*, pp. 1–13, 2015.
- [37] N. Kanwisher and G. Yovel, “The fusiform face area: a cortical region specialized for the perception of faces.,” *Philos. Trans. R. Soc. Lond. B. Biol. Sci.*, vol. 361, no. 1476, pp. 2109–28, 2006.
- [38] J. D. Yeatman, K. S. Weiner, F. Pestilli, A. Rokem, A. Mezer, and B. A. Wandell, “The vertical occipital fasciculus: A century of controversy resolved by in vivo measurements,” *Proc. Natl. Acad. Sci.*, vol. 111, pp. E5214–E5223, dec 2014.

5. GROUPWISE STRUCTURAL PARCELLATION OF THE WHOLE CORTEX: A LOGISTIC  
RANDOM EFFECTS MODEL BASED APPROACH

---

# Chapter 6

## Solving the Cross-Subject Parcel Matching Problem using Optimal Transport

---

### 6.1. Overview

Matching structural parcels across different subjects is an open problem in neuroscience. Even when produced by the same technique, parcellations tend to differ in the number, shape, and spatial localization of parcels across subjects. In this chapter, we propose a parcel matching method based on Optimal Transport. We test its performance by matching parcels of the Desikan atlas, parcels based on a functional criteria and structural parcels. We compare our technique against three other ways to match parcels which are based on the Euclidean distance, the cosine similarity, and the Kullback-Leibler divergence. Our results show that our method achieves the highest number of correct matches.

### 6.2. Introduction

Brain organization displays high variability across individuals and species. Studying brain connectivity therefore faces the challenge of locating homogeneous regions while accounting for this variability. Different techniques have been proposed to parcelate the brain based on its structural connectivity. However, matching the resulting parcels across different subjects is still an open problem in neuroscience. Even when produced by the same technique, parcellations tend to differ in the number, shape, and spatial localization of parcels across subjects<sup>1</sup>. Current theories hold that long-range structural connectivity, namely, extrinsic connectivity, is strongly related to brain function<sup>2</sup>. Therefore, being able to match parcels with similar connectivity across subjects can help to understand brain function while also enabling the comparisons of cortical areas across different species<sup>3</sup>.

Most of the current methods to match parcels across subjects are strongly linked to the tech-

nique used to create them. For example, Moreno-Dominguez et al.<sup>4</sup> seek correspondences between dendograms created by means of Hierarchical Clustering. Parisot et al.<sup>5</sup> impose the consistency of parcels across subjects while creating the parcellation. In recent works Mars et al. propose to use the Manhattan distance, cosine similarity<sup>6</sup> or the KullbackLeibler (KL) divergence<sup>3</sup> to compare and match connectivity fingerprints, successfully identifying common areas across humans and primates.

In this work, we propose to match parcels based on their extrinsic connectivity fingerprint using Optimal Transportation theory. Optimal Transport (OT) is a technique that seeks the optimal way to transport mass between probability distributions. While KL divergence computes the difference between two distributions, OT computes a matching between them. In particular, our method adopts a discrete regularized version of Optimal Transport (OT), which has been presented in Gayraud et al.<sup>?</sup> and Courty et al.<sup>?</sup> as a solution to the domain adaptation problem.

We validate our method with four different experiments. In the first experiment, we test the feasibility of our method by generating parcels with synthetic connectivity fingerprints and matching them. In the second one, we show that our technique is able to match parcels of the same atlas across subjects. We use the anatomical atlas of Desikan<sup>7</sup> as its parcels have high spatial coherence and consistent connectivity profiles across subjects<sup>8</sup>. Finally, we show the capacity of our method to match parcels generated with the same criteria but have some spatial cross-subject variability. We assess this for two different situations. In the first one, we derive the parcels from functional activations<sup>9</sup>. We use responses to motor and visual stimuli since they have been shown to be strongly related to structural connectivity<sup>10,11</sup>. In the second one, we di-

## 6. SOLVING THE CROSS-SUBJECT PARCEL MATCHING PROBLEM USING OPTIMAL TRANSPORT

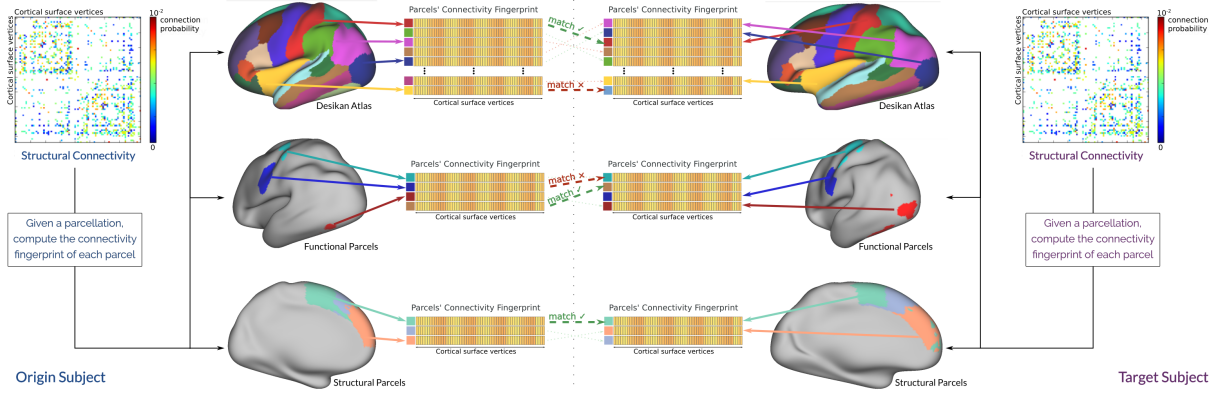


**Figure 6.1:** From the cortico-cortical structural connectivity matrix of a subject, we can estimate the connectivity fingerprints of each parcel in three different types of parcellations. For each parcellation we compute the amount of correct matches (green lines) that each matching technique produces.

vide the Lateral Occipital Gyrus in 3 parcels using a structurally-based parcellation technique<sup>12</sup>. We use the Lateral Occipital Gyrus since it has been shown to have a consistent parcellation across subjects<sup>13;12</sup>. The outline of the last three experiments can be seen in Figure 6.1.

In each experiment, we compare our technique against three other ways to match parcels based on the Euclidean distance; the cosine similarity; and the Kullback-Leibler divergence. Our results on real data show that our method based on OT always achieves the highest number of correct matches.

### 6.3. Methods

Given two subjects with their respective parcellations, we compute their parcel matching by considering one as the origin and the other one as target. More formally, let  $X^a = \{x_i^a\}_{i=1}^{N_a}$ ,  $x_i^a \in \Omega^a \subset \mathbb{R}^n$  be an origin dataset where  $N_a$  denotes the number of parcels;  $x_i^a$  is the extrinsic connectivity fingerprint of parcel  $i$ ; and  $n$  denotes its dimension. We wish to recover a matching between  $X^a$  and a target dataset  $X^b = \{x_i^b\}_{i=1}^{N_b}$ ,  $x_i^b \in \Omega^b \subset \mathbb{R}^n$ .

In this section, we start by formulating our regularized discrete OT-based method and proceed by presenting three ways of computing this matching that are based on the Euclidean distance; the cosine similarity; and the KL-divergence.

### Discrete Regularized Optimal Transport

Optimal Transport (OT) theory boils down to finding the optimal way to transport or redistribute mass from one probability distribution to another with respect to some cost function. In this work, since the datasets  $X^a$  and  $X^b$  are discrete datasets, we use their empirical probability distributions and apply the discrete formulation of OT<sup>7,8</sup> to solve the parcel matching problem. A simplified example of how our method proceeds is presented in Figure 6.2.

Assume that  $X^a$  and  $X^b$  follow probability distributions  $p_a(x^a)$  and  $p_b(x^b)$ , respectively. We suppose that  $X^a$  has undergone a transformation  $\mathbf{T} : \Omega^a \rightarrow \Omega^b$ , such that  $p_b(\mathbf{T}(x^a)) = p_b(x^b)$ . We wish to recover  $\mathbf{T}$  and use it to match the parcels of  $X^a$  and  $X^b$ . Using discrete regularized OT we compute a transport plan  $\gamma_0$  between these two probability distributions. This transport plan is a doubly stochastic matrix which minimizes a certain transportation cost  $C$  over the vectors of  $X^a$  and  $X^b$ . In other words, it defines the optimal exchange of mass between the two probability distributions. We use  $\gamma_0$  to compute an estimation  $\hat{\mathbf{T}}$  by selecting the pairs of vectors, i.e., parcels that exchange the most mass.

Since  $p_a(x^a)$  and  $p_b(x^b)$  are not known, we use the corresponding empirical distributions  $\mu_a = \sum_{i=1}^{N_a} p_i^a \delta_{x_i^a}$  and  $\mu_b = \sum_{j=1}^{N_b} p_j^b \delta_{x_j^b}$  instead, where  $p_i^a$  and  $p_j^b$  are the probability masses associated to each sample. However, given that the dimension of

## 6. SOLVING THE CROSS-SUBJECT PARCEL MATCHING PROBLEM USING OPTIMAL TRANSPORT

---

our data depends on the number of vertices in the cortical mesh, the curse of dimensionality makes the estimation of  $\mu_a$  and  $\mu_b$  intrinsically difficult. We therefore simply assume a uniform probability distribution over all vectors,  $p_i^a = \frac{1}{N^a}$  and  $p_j^b = \frac{1}{N^b}$ . We compute the transport plan  $\gamma_0$  such that, if

$$\mathcal{B} = \left\{ \gamma \in (\mathbb{R}^+)^{N_a \times N_b} \mid \gamma \mathbf{1}_{N_b} = \frac{1}{N^a} \mathbf{1}_{N_a}, \gamma^T \mathbf{1}_{N_a} = \frac{1}{N^b} \mathbf{1}_{N_b} \right\} \quad (6.1)$$

denotes the set of all doubly stochastic matrices whose marginals are the probability measures  $\mu_a$  and  $\mu_b$ , where  $\mathbf{1}_N$  is an  $N$ -dimensional vector of ones, then  $\gamma_0 \in \mathcal{B}$  is the output of the following minimization problem.

$$\gamma_0 = \arg \min_{\gamma \in \mathcal{B}} \langle \gamma, C \rangle_F + \lambda \sum_{i,j} \gamma(i,j) \log \gamma(i,j) \quad (6.2)$$

The matrix  $C$ , where  $C(i,j) = \|x_i^a - x_j^b\|_2^2$ , represents the cost of moving probability mass from location  $x_j^a$  to location  $x_i^b$ , in terms of their squared Euclidean distance. The rightmost term is a regularization term based on the negative entropy of  $\gamma$  allows us to solve this optimization problem using the Sinkhorn-Knopp algorithm<sup>7</sup> which improves the computation time.

Matrix  $\gamma_0$  contains information about the exchange of probability mass between the vectors of  $X^a$  and  $X^b$ . By construction, this exchange depends on the selected cost function. The choice of the squared euclidean distance is motivated both by the fact that it renders the optimization problem convex and because it will allow the parcels to be matched according to the vicinity of their feature vectors. Hence, the origin feature vectors will distribute their corresponding probability mass to the target feature vectors that are closest to them. Consequently, we define  $\hat{\mathbf{T}} : \Omega^a \rightarrow \Omega^b$  as  $\hat{\mathbf{T}}(x_i^a) = x_{\hat{j}}^b$  where  $\hat{j} = \arg \max_j \gamma_0(i,j)$ . Therefore,  $i$  will be matched to the parcel  $\hat{j}$  that it sent the most mass to.

### Matching Parcels Based on Dissimilarity Between Features

Let  $d(x_i^a, x_j^b)$  be some dissimilarity measure between the elements of  $X^a$  and  $X^b$ . Then,

we say that parcel  $i$  matches parcel  $j$  if  $\arg \min_k d(x_i^a, x_k^b) = j$ . We compare three dissimilarity measures against our method. First, we use the Euclidean distance, which can be interpreted as matching the parcel  $i$  to the parcel  $j$  whose feature vector  $x_j^b$  is the closest to  $x_i^a$ . Then, we use the cosine similarity, which is minimized when two feature vectors are colinear. Lastly, we use the Kullback-Leibler divergence, which measures the difference between two probability distributions in terms of their relative entropy. Note that we need to convert our vectors into probability vectors in order to evaluate  $d_{KL}$ .

## 6.4. Experiments and Results

---

### Data and Preprocessing

For this work we randomly selected 20 subjects from the S500 group of the Human Connectome Project (HCP), all preprocessed with the HCP minimum pipeline<sup>14</sup>. Fiber orientation distributions functions were computed using spherical constrained deconvolution with a spherical harmonic order of 8. Probabilistic tractography was then performed using 1000 seeds per vertex of the cortical mesh provided with the HCP data. For each subject, we computed a connectivity matrix by counting the number of streamlines that connect each pair of vertices of the cortical mesh. Each row in the matrix is a vertex connectivity vector, representing the probability that a connection exists between a surface vertex and the rest of the surface's vertices.

Given a whole brain cortical parcellation, we compute the connectivity fingerprint of each parcel by averaging the connectivity fingerprint of its vertices. Because the mesh's vertices are coregistered across subjects<sup>14</sup>, we are able to compare the connectivity fingerprints across subjects. The criterion to compute the parcel matching between two subjects is the similarity between connectivity fingerprints. That is, we match two parcels if they are connected to the rest of the brain in a similar manner. Due to the distance bias that occurs in tractography, a parcel tends to be highly connected to the vertices that compose it. To prevent the matching to be influenced by this bias, we disconnect each parcel from its own vertices.

## 6. SOLVING THE CROSS-SUBJECT PARCEL MATCHING PROBLEM USING OPTIMAL TRANSPORT

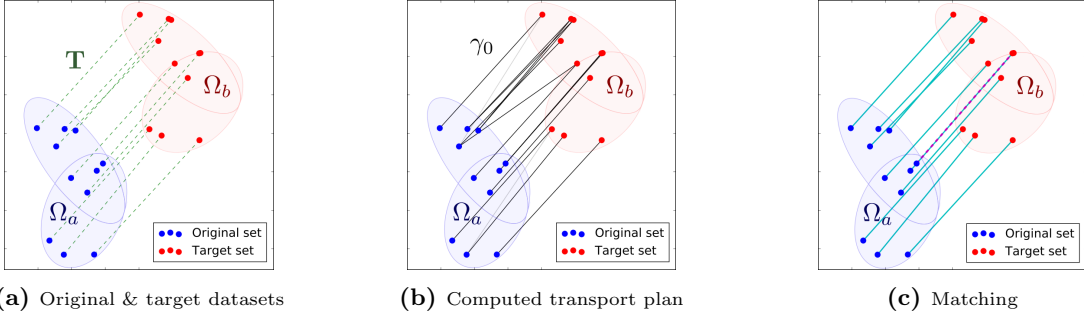


**Figure 6.2:** A 2-d example of using OT to compute the matching between two different datasets. On the left we show the original and target datasets. The real matchings are displayed as green dashed edges. In the middle, the edge densities represent the values of the computed coupling  $\gamma_0$ , which denote the amount of mass that is exchanged between vectors  $x_i^a$  and  $x_j^b$ . On the right, we see the recovered matching. The blue edges represent the correct matchings, while the red dotted edges represent the incorrect ones.

### Matching Parcels

In this section we evaluate the performance of our method by comparing it to the methods presented in Section 6.3.2. For each experiment we compute parcel matchings between all possible pairs of connectivity matrices. To quantify the result of each technique, we compute the accuracy in terms of percentage of correctly matched parcels per pairwise matching.

#### Matching parcels with synthetic fingerprints.

In this first experiment, we test the feasibility of our method by generating parcels with synthetic connectivity fingerprints and matching them. We start by generating a connectivity matrix  $M$  using probabilistic Constrained Spherical Deconvolution based tractography to use as ground truth. Our ground truth matrix is a square matrix that represents the connectivity between the 64 parcels of the Desikan atlas in one subject of the HCP dataset. Each coefficient  $M(i, j) = \theta_{ij}$  is the parameter of a random variable that follows a Bernoulli distribution  $X_{ij} \sim B(\theta_{ij})$ . This variable  $X_{ij}$  represents the probability of a connection existing between the parcels  $i$  and  $j$ . Using  $M$ , we generate 20 synthetic matrices in such a way that the coefficients of each synthetic connectivity matrix are random variables that follow a binomial distribution  $X(i, j) \sim B(p = M(i, j), n)$ . By doing this we simulate doing tractography for various values of the number  $n$  of particles. Figure 6.3a shows the

performance of each method as a function of  $n$ .

#### Matching parcels of the Desikan Atlas.

For each subject, we compute the connectivity fingerprint of each parcel in their Desikan atlas as explained in Section 6.4.1. When matching parcels across subjects, Figure 6.3b shows that on average OT achieves an accuracy of  $98\% \pm 2\%$ , followed by cosine similarity ( $94\% \pm 3\%$ ), KL divergence ( $87\% \pm 4\%$ ), and finally Euclidean distance ( $77\% \pm 11\%$ ).

#### Matching parcels created using functional criteria.

Each subject in the HCP dataset possesses z-score maps representing responses to different stimuli obtained with functional MRI (fMRI)<sup>9</sup>. We derive parcels for each subject from the responses to motor (hand, foot and tongue movement) and visual stimuli (faces vs shape recognition). We do so by keeping only the vertices whose z-score is in the top 35%. Figure 6.3b shows that OT performs best with an average of  $98\% \pm 6\%$ . The cosine similarity, KL divergence, and Euclidean distance achieve average accuracies of  $97\% \pm 6\%$ ,  $92\% \pm 10\%$ , and  $90\% \pm 13\%$  respectively.

## 6. SOLVING THE CROSS-SUBJECT PARCEL MATCHING PROBLEM USING OPTIMAL TRANSPORT

---

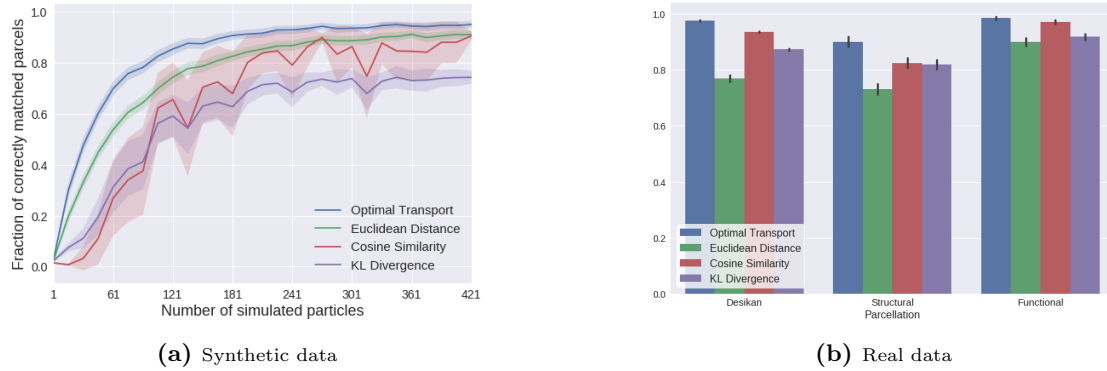


**Figure 6.3:** Proportion of parcels correctly matched by each method (see section 6.3.2) when matching: (a) synthetic connectivity fingerprints and (b) connectivity fingerprints of a cortical parcellation, for three different parcellations (as described in section 6.4.2). OT always performs significantly better.

### Matching parcels created using structural criteria.

For each subject, we first mask their Lateral Occipital Gyrus using the Desikan atlas. Then, we divide it into 3 parcels using the structural based parcellation technique of Gallardo et al.<sup>12</sup>. Once more, we can see on Figure 6.3b that optimal transport has the highest average accuracy, equal to  $92\% \pm 16\%$ . It is followed by the cosine similarity, the KL divergence, and the Euclidean distance, whose average accuracies equal  $85\% \pm 17\%$ ,  $84\% \pm 17\%$ , and  $75\% \pm 17\%$ .

## 6.5. Discussion

In this work we proposed a method to match parcels across subjects based on the connectivity fingerprint of a parcel.

We tested our method with four different experiments. In the first experiment our technique correctly matched connectivity fingerprints created in a synthetic way. Specifically, each entry in a fingerprint was sampled from a Binomial distribution, whose parameter was chosen as the corresponding value of a ground truth connectivity matrix. This can be thought as a simulation of the process of tracking in tractography with different number of streamlines.

Our second experiment shows that we can correctly match parcels of the Desikan atlas across sub-

jects with a 98% of correct matches. The parcels of the Desikan atlas are known to have high spatial coherence and consistent connectivity profiles across subjects<sup>8</sup>. We therefore use this experiment as a reference point to benchmark our technique. The last two experiments show that our technique can match parcels generated with a same criteria, even when they have some spatial variability across-subjects. The first experiment uses parcels created from the functional response to specific motor and visual stimuli, known to be strongly linked to functional connectivity<sup>10;11</sup>. The second one, parcels created from the structural parcellation of the Lateral Occipital Gyrus, a structure documented to have a consistent structural division<sup>13;12</sup>.

It's important to notice that our technique achieved more than a 90% of correct matches in every experiment with real data. Given that we used 20 subjects, this represents a total of  $20 \times 19 = 380$  cross-subject matches. In the case of the Desikan atlas, which possesses 64 parcels, this translates into a total of 24320 matches, from which 98% were correctly matched. Furthermore, when tested with a paired t-test to compare the number of correct matches, our method always performs significantly better than the other three ( $p < 10^{-256}$ ).

## 6. SOLVING THE CROSS-SUBJECT PARCEL MATCHING PROBLEM USING OPTIMAL TRANSPORT

---

### 6.6. Conclusion

Matching structural parcels across different subjects is an open problem in neuroscience. In this work, we proposed a novel parcel matching method based on Optimal Transport. We tested its performance with four different experiments, always obtaining the highest number of correctly matched parcels, which is an improvement over the results of the currently used techniques. Our technique could have major implications in the study of brain connectivity and its relationship with brain function, allowing for the location of parcels with similar connectivity but not high spatial coherence. Also, it could help to understand the link between different brain atlases, and improve the comparisons of cortical areas between higher primates.

### Bibliography

---

- [1] S. Jbabdi and T. E. Behrens, “Long-range connectomics,” *Ann. N. Y. Acad. Sci.*, vol. 1305, pp. 83–93, dec 2013.
- [2] R. E. Passingham, K. E. Stephan, and R. Kotter, “The anatomical basis of functional localization in the cortex,” *Nat. Rev. Neurosci.*, vol. 3, pp. 606–616, aug 2002.
- [3] R. B. Mars, S. N. Sotiropoulos, and R. E. Passingham, “Whole brain comparative anatomy using connectivity blueprints,” *bioRxiv*, p. 245209, 2018.
- [4] D. Moreno-Dominguez, A. Anwander, and T. R. Knösche, “A hierarchical method for whole-brain connectivity-based parcellation,” *Hum. Brain Mapp.*, vol. 35, pp. 5000–5025, oct 2014.
- [5] S. Parisot, S. Arslan, J. Passerat-Palmbach, W. M. Wells, and D. Rueckert, “Tractography-Driven Groupwise Multi-scale Parcellation of the Cortex.,” *Inf. Process. Med. Imaging*, vol. 24, pp. 600–12, 2015.
- [6] R. B. Mars, L. Verhagen, T. E. Gladwin, F. X. Neubert, J. Sallet, and M. F. S. Rushworth, “Comparing brains by matching connectivity profiles,” *Neurosci. Biobehav. Rev.*, vol. 60, pp. 90–97, 2016.
- [7] R. S. Desikan, F. Ségonne, B. Fischl, B. T. Quinn, B. C. Dickerson, D. Blacker, R. L. Buckner, A. M. Dale, R. P. Maguire, B. T. Hyman, M. S. Albert, and R. J. Killiany, “An automated labeling system for subdividing the human cerebral cortex on MRI scans into gyral based regions of interest,” *Neuroimage*, vol. 31, pp. 968–980, jul 2006.
- [8] M. A. de Reus and M. P. van den Heuvel, “The parcellation-based connectome: Limitations and extensions,” *Neuroimage*, vol. 80, pp. 397–404, 2013.
- [9] D. M. Barch, G. C. Burgess, M. P. Harms, S. E. Petersen, B. L. Schlaggar, M. Corbetta, M. F. Glasser, S. Curtiss, S. Dixit, C. Feldt, D. Nolan, E. Bryant, T. Hartley, O. Footer, J. M. Bjork, R. Poldrack, S. Smith, H. Johansen-Berg, A. Z. Snyder, and D. C. Van Essen, “Function in the human connectome: Task-fMRI and individual differences in behavior,” *Neuroimage*, vol. 80, pp. 169–189, oct 2013.
- [10] D. E. Osher, R. R. Saxe, K. Koldewyn, J. D. E. Gabrieli, N. Kanwisher, and Z. M. Saygin, “Structural Connectivity Fingerprints Predict Cortical Selectivity for Multiple Visual Categories across Cortex,” *Cereb. Cortex*, vol. 26, no. 4, pp. 1668–1683, 2016.
- [11] W. Penfield and H. Jasper, *Epilepsy and the Functional Anatomy of the Human Brain*. 1954.
- [12] G. Gallardo, W. Wells, R. Deriche, and D. Wassermann, “Groupwise structural parcellation of the whole cortex: A logistic random effects model based approach,” *Neuroimage*, pp. 1–14, feb 2017.
- [13] M. Thiebaut de Schotten, M. Urbanski, B. Battocourt, R. Levy, B. Dubois, L. Cerliani, and E. Volle, “Rostro-caudal Architecture of the Frontal Lobes in Humans,” *Cereb. Cortex*, pp. 1–15, 2016.
- [14] M. F. Glasser, S. N. Sotiropoulos, J. A. Wilson, T. S. Coalson, B. Fischl, J. L. Andersson, J. Xu, S. Jbabdi, M. Webster, J. R. Polimeni, D. C. Van Essen, and M. Jenkins, “The minimal preprocessing pipelines for

## 6. SOLVING THE CROSS-SUBJECT PARCEL MATCHING PROBLEM USING OPTIMAL TRANSPORT

---

the Human Connectome Project,” *Neuroimage*, vol. 80, pp. 105–124, oct 2013.

6. SOLVING THE CROSS-SUBJECT PARCEL MATCHING PROBLEM USING OPTIMAL  
TRANSPORT

---

# Chapter 7

## Inferring the Localization of White-Matter Tracts using Diffusion Driven Label Fusion

---

### 7.1. Overview

In the previous chapters we studied the structural organization of the brain, and saw that it is highly related to function. We also talk, specifically in chapter X, about how lesions in the cortex or white matter disrupt the normal functioning of the brain. Some white matter pathologies, such as tumors or traumatic brain injury, affect the white matter to the point where it's difficult to even infer which pathways are affected using tractography. In this chapter, we introduce a way to infer the location of pathways, even when it's not possible to use tractography to locate them. Our technique is based on a methodology named label fusion. In particular, we show how to add dMRI information to the label fusion in order to better estimate the location of white matter pathways.

### 7.2. Introduction

White matter pathologies such as tumors or traumatic brain injury disrupt the structure of white matter. These disruptions hamper the inference of affected pathways using tractography. Furthermore, for some pathologies as tumors or edemas, estimating brain pathways using tractography becomes impossible [cite]. For such pathologies, it's not possible to use Diffusion Magnetic Resonance Imaging (dMRI) to tract within or around the lesion. Given the nature of the lesions, the tracking results in interrupted or erroneous tracts. This situation makes hard to infer which pathways are directly affected by the pathology. One possible way to overcome this issue, is by aggregating spatial information from other subjects in order to infer the affected tracts. Assuming we know the location of a set of tracts in the brains of a group of healthy subjects, we could register them to the brain of our patient and use a label fusion technique. Label fu-

sion is a family of techniques that aims to infer the localization of the brain structure of a subject from its localization in a group of control subjects. One well known technique within this family is Majority Voting [cite]. Given a specific location, each subject is said to "vote" for one label. The inferred label for that location will be the one with more votes. For example, when labeling a volume, each voxel receives the label voted by the majority of the control subjects.

Majority Voting is simple to implement and has been demonstrated to yield accurate segmentations [reference]. However, this technique is blind both to registration problems and anatomical variability between subjects. To overcome this, it has been proposed to weight the vote of each subject by some measure of similarity between the patient and the subject [cite]. The underlying intuition is that the choosing of labels should be driven by those subjects who resemble the most to the one being labeled. The practical advantages of various strategies based on this idea have recently been demonstrated [6-sabuncu].

The techniques described so far rely only on anatomical information, not taking into account the structure of white matter. In the case of white matter pathways, the presence of a path constrains the Brownian motion in the brain, which can be measured by dMRI. In this work, we introduce a new label fusion technique that, taking advantage of dMRI, weights the vote of each subject based on how the voted pathway is supported by the test subject's diffusion data. This is, if the diffusion data of the test subject is consistent with the direction of the voted pathway, the vote has a higher weight. Our technique also allows to work with crossing tracts, by modeling multiple labels per voxel.

We validate our technique in 13 subjects of the Human Connectome Project (HCP). For each subject,

## 7. INFERRING THE LOCALIZATION OF WHITE-MATTER TRACTS USING DIFFUSION DRIVEN LABEL FUSION

---

we infer the location of 18 left hemisphere tracts using whole-brain tractography and an implementation of the white matter query language (WMQL). We use this results as ground truth to compare against inferring the tracts from using the other 12 subjects with our proposed technique and Majority Voting. Our results show that adding dMRI to the label fusion process achieves a similar number of true positives than Majority Voting, with a 60% less of false positives, incurring in a trade-off of a 40% false negatives.

### 7.3. Methods

---

Our label fusion technique takes advantage of dMRI to weight the vote of each subject. The vote for a specific label gets a higher weight if it's supported by the diffusion data of the subject being labeled. In this section, we first start explaining the concept of Orientation Density Function of diffusion in dMRI and tract directionality. Then, we present how to use these concepts to compute the weights of each vote.

#### Estimating an Orientation Density Function

A dMRI image is composed by many volumes, each one linked to an acquisition direction. Each value in these volumes represents the intensity of diffusion in that point of the brain for the direction linked to the volume. By fitting the diffusion information of a voxel in a Constrained Spherical Deconvolution model, it's possible to estimate a orientation density function (ODF) over a sphere. Needs more explanation.

#### Estimating an Orientation Density Function

Given a tract expressed as set of streamlines, assuming they don't have sharp turns we can estimate their main directionality on a voxel by looking at its entry and exit points. For each pair of entry and exit points we can compute a direction, and from this set of directions, we can compute a ODF over a sphere, expressing the distributions of directions for that voxel. Explain ACGD.

#### Label fusion

In the previous section we presented how to compute and ODF from dMRI data and how to estimate the ODF from a tract in a voxel. Now, we introduce the Majority Voting technique and our improvement using dMRI.

#### Majority Voting

Let  $\text{labels} = \{l_i\}, \forall i l_i \in N$  be the set of labels representing tracts and grey matter structures in one hemisphere. Let  $L_s, s \in S$  represent the labeling of a set of subjects  $S$ , where each  $L_s \in \text{labels}^{v \times v}$  is a 3D volume representing the labeling of a specific subject. Majority Voting [Rohlfing et al. (2004)] infers the label of each voxel  $x$  in the test subject ( $L(x)$ ) by computing:

$$\hat{L}(x) = \arg \max_{l \in \text{labels}} \sum_{s \in S} p(L(x) = l | L_s(x)),$$

where

$$p(L(x) = l | L_s(x)) = \begin{cases} 1, & \text{if } L_s(x) = l \\ 0, & \text{otherwise} \end{cases} \quad (7.1)$$

In this case, it's said that each train subject votes for a label per voxel, and the label with the most amount of votes is assigned to the test subject's voxel.

#### Diffusion based label fusion

We want to introduce a weight to these votes, taking into account how well the tract can explain the underlying Diffusion data of our test subject. In particular, we want to the Orientation Distribution Function (ODF) of our test subject's diffusion. This is, we want to profit of the fact that we know how the water particles are moving in its brain, following the underlying tracts. As explained in section X, in a given voxel, we can compute the main directionality of the tract  $l$  of the train subject  $s$  and the ODF of our test subject's diffusion. To see if the tract are aligned with the directionality of the voted tract we proposed the following model:

## 7. INFERRING THE LOCALIZATION OF WHITE-MATTER TRACTS USING DIFFUSION DRIVEN LABEL FUSION

---

$$\hat{L}(x) = \arg \max_{l \in \text{labels}} \sum_{s \in S} p(L(x) = l; L_s(x)) p(D(x); P_{\text{he}}(x)) \quad (7.2)$$

where

$$p(P(x); D_{sl}(x)) = \langle ODF(x), ODF_{sl}(x) \rangle. \quad (7.3)$$

In our model, the first term remains the same as in the voting scheme. Our second term,  $p(D(x)|D_{sl}(x))$  express the probability of seeing the ODF that we found in our test subject, given that the real tract passing by is the one voted by the test subject. We compute this probability as in [REFERENCE], by computing the inner product between the two ODFs. The ODFs need to be first normalized in order for  $\|ODF_i\|_2 = 1$ .

In the case of multi-label, we can combine the info of directions in a same acgd. This allows us to better compute the real label when there are fibers crossing inside of a voxel. For each voxel in the white-matter of our test subject, we select the label with the highest summation of weighted votes.

### 7.4. Experiments and Results

---

In the previous section we presented how to add Diffusion weighted information to the process of Majority Voting in order to improve the multi-atlas technique. Now, we present experiments, both in synthetic and real data, showing that our technique achieves better results than Majority Voting.

#### Data and Preprocessing

We randomly selected 13 subjects from the HCP500 dataset from the Human Connectome Project. For each subject, we computed whole-brain tractography using each voxel in the white-matter as a seed and simulating 8 particles per seed [REF]. We extracted the main tracts from the left hemisphere tractogram (18 tracts in total) using the implementation of the white-matter query language (WMQL),(Wasserman et al. 2016). For each pair of subjects, we registered their tracts to each other's brain.

#### Assessing goodness of the technique in syn-

#### thetic data

$P_{\text{he}}(x)$  dwi of TEST has one tract. We have two types of subjects, ST who votes for a tract, and S0 who votes for no tracts. ST starts with a completely aligned tract, and we rotate it until 90 deg. Then, we compute the weight of each vote. The proportion between them, tells us how many subjects we need to get either one or the other label. We show that, when we have subjects voting for the right tract, their weight goes up, allowing to only 30% of them to win. But when the tract is not aligned, then they lose, except if they're the 70%. In between.. stuff. But, when the GT is NO-TRACT, we always need more than 60% of the people. Something similar happens with crossing, I hope. This is better than the 50% of voting.

#### Assessing goodness of the techniques in real data

To assess the "goodness" of our technique we made a leave-one-out cross-validation. At each step, we selected one of the subjects as test and used the rest as train subjects. Using the registered tracts of the train subjects, we computed parcellations using both the voting rule and our technique. Since we also have the tracts of each test subject, we compute a 'ground truth' parcellation of the white matter. Finally, we computed the confusion matrix of both the Majority Voting and our technique. A confusion matrix is a matrix of size labels by labels where the entry (i,j) is the number of times the label in the ground truth was i and the technique labeled j. Table 1 shows that our proposed achieves a similar number of false negatives while obtaining a 64% less of false positives in average. This incurs on a trade-off of having 39% more false negatives and 18% less true positives in average, underlying that our technique is more conservative.

#### Simulating Lesions in the White-Matter

To test how our technique would behave in an injured brain, we simulate a tumor in the white matter of one of our subjects. We place the tumor to interrupt the ILF. We do so by selecting a set of neighboring voxels where the ILF passes by, and

## 7. INFERRING THE LOCALIZATION OF WHITE-MATTER TRACTS USING DIFFUSION DRIVEN LABEL FUSION

---

mix their signal with diffusion signal from random voxels in the ventricles. This is, for each selected voxel  $x$  in the brain, we chose a random voxel  $v$  in the ventricle and mix their signals:

$$S(x) = S(x)(1 - \alpha) + S(v)\alpha, \alpha \in [0, 1]$$

. Since the ventricles are regions filled with cerebrospinal fluid (CSF), they diffusion is approximately isotropic. We compute for which values of  $\alpha$  WMQL stops being able to detect the ILF, and for which values our technique stops being able to detecting it. Since the Major Voting does not rely on diffusion data, this experiment does not affect the results obtained in the previous experiment for Major Voting. WMQL stops detecting the ILF at.... and our technique stops detecting it in the voxels at ....

### Discussion

We want to infer the position of tracts in the white matter. Since we do not have many subjects, we cannot relay on Deep Learning techniques. We decide to use Label Fusion techniques. Some people showed that Majority Voting works well for this things. The problem is that majority voting relies only on the spatial location. Problems of registration. We introduce a new way to take into account the diffusion information. This makes a lot of sense, since we are trying to infer tracts, and the diffusion data is related to the underlying tracts. In synthetic data, we show that our technique is much better than majority voting, specially when the tracts align correctly with the underlying diffusion. It also works like charm, when the tracts are completely missaligned with the diffusion. In other cases, is as good as majority voting. In real data, this is reflected, by showing that diffusion voting is more conservative. WMM lessons.

### Conclusions

In this chapter we presented a labeling fusion technique that relies on dMRI data to infer the localization of white-matter tracts. The results show that our technique is more conservative than the voting rule, which is desired when studying pathologies, at the cost of having more false negatives.

**Table 7.1:** Confusion matrix for both techniques and the ratio between them

	Diffusion		Voting		Ratio
	Background	Tract	Background	Tract	
Background	3658350	11849	3568123	24619	1.48
Tract	27932	2592	17050	3163	0.86

### Table

Figure 1. Outline of our technique. We extract the main white-matter tracts using WMQL, register them to the 'test' subject and then compute a voting rule weighted by diffusion information. For each voxel  $x$  in the 'test' subject, we select the label  $l$  that maximizes equation 7.2, where  $S$  is the set of 'train' subjects,  $t$  is the 'test' subject;  $L_i(x)$  is the label of voxel  $x$  for the subject  $i$ ;  $P$  are the principal directions of diffusion in the 'test' subject and  $D_{sl}(x)$  are the directions of tract  $l$  in the voxel  $x$  of the 'train' subject  $s$ .

### Bibliography

---